INL/JOU-17-41167
Accepted Manuscript

TEM characterization of irradiated U-7Mo/Mg dispersion fuel

J. Gan, D. D. Keiser, B. D. Miller,
J. F. Jue, A. B. Robinson, J. Madden

October 2017

The INL is a
U.S. Department of Energy
National Laboratory
operated by
Battelle Energy Alliance

Prepared for the U.S. Department of Energy
Office of Nuclear Energy
Under DOE Idaho Operations Office
Contract DE-AC07-05ID14517

Journal of Nuclear Materials xxx (2017) 1–18

Contents lists available at ScienceDirect

Journal of Nuclear Materials

journal homepage: www.elsevier.com/locate/jnucmat

TEM characterization of irradiated U-7Mo/Mg dispersion fuel

J. Gan*, D.D. Keiser Jr., B.D. Miller, J.F. Jue, A.B. Robinson, J. Madden

Advanced PIE and Characterization Division, Idaho National Laboratory, P. O. Box 1625, Idaho Falls, ID 83415-6188, USA

ARTICLE INFO

Article history:
Received 13 March 2017
Received in revised form
13 July 2017
Accepted 14 July 2017
Available online xxx

Keywords:
Dispersion fuel
TEM
Mg matrix
U-7Mo
Fission
Microstructure

ABSTRACT

This paper presents the results of transmission electron microscopy (TEM) characterization on neutron-irradiated samples taken from the low-flux and high-flux sides of the same fuel plate with U-7Mo fuel particles dispersed in Mg matrix with aluminum alloy Al6061 as cladding material that was irradiated edge-on to the core in the Advanced Test Reactor. The corresponding local fission density and fission rate of the fuel particles and the average fuel-plate centerline temperature for the low-flux and high-flux samples are estimated to be 3.7×10^{21} f/cm^3, 7.4×10^{14} f/cm^3/s and 123 °C, and 5.5×10^{21} f/cm^3, 11.0×10^{14} f/cm^3/s and 158 °C, respectively. Complex interaction layers developed at the Al-Mg interface, consisting of Al_3Mg_2 and $Al_{12}Mg_{17}$ along with precipitates of MgO, Mg_2Si and $FeAl_{5.3}$. No interaction between Mg matrix and U-Mo fuel particle was identified. For the U-Mo fuel particles, at low fission density, small elongated bubbles wrapped around the clean areas with a fission gas bubble superlattice, which suggests that bubble coalescence is an important mechanism for converting the fission gas bubble superlattice to large bubbles. At high fission density, no bubbles or porosity were observed in the Mg matrix, and pockets of residual fission gas bubble superlattice were observed in the U-Mo fuel particle interior.

Published by Elsevier B.V.

1. Introduction

The former Reduced Enrichment Research and Test Reactor (RERTR) fuel program, currently called the Materials Minimization and Management (M3) fuel program, is developing low enrichment fuels (<20% U-235) for research and test reactors around the world [1–3]. The plate type dispersion fuel with U(Mo) fuel particles dispersed in Al alloy matrix is a popular fuel form. It is known that the extensive interaction occurs between the U-Mo fuel and aluminum alloy matrix, which results in the development of phases that could have detrimental effects on fuel performance [4–6]. Various approaches have been employed to mitigate the fuel-matrix-interaction (FMI) including adding Si in Al matrix or applying a thin Si or ZrN ceramic coating to minimize the diffusion reaction between the U-Mo fuel particle and matrix [7–11]. Both FMI and the irradiated microstructure of U-Mo fuel could have significant impact on fuel performance. When choosing the matrix material, it should have the following properties of low neutron absorption, inert to chemical reaction with fuel alloy, a high melting point, good thermal conductivity, good compatibility with the cladding, low solubility in the coolant, and good mechanical properties. While aluminum alloy matrix is considered a primary option for low enrichment fuel for research and test reactors, Mg matrix may be considered an alternative as a result of its low thermal neutron absorption, no chemical interaction with U-Mo fuel alloy, good compatibility with Al cladding and good compatibility with fuel plate fabrication process similar to what are used for Al matrix fuels. A comprehensive review of the previous work on Mg matrix U-Mo dispersion fuel can be found in a recent publication by Keiser et al. on scanning electron microscopy (SEM) investigation of the same U-7Mo/Mg dispersion mini fuel plate (ID: R9R010) irradiated as part of RERTR-8 irradiation campaign at the Advanced Test Reactor (ATR) at Idaho National Laboratory [12]. This paper presents the recent transmission electron microscopy (TEM) results that complement the reported SEM results.

No data on the TEM characterization of neutron irradiated U-7Mo/Mg fuel has been found in the literature. Chiang et al. performed TEM and micro x-ray diffraction (μ-XRD) characterization of U(Mo)/Mg dispersion fuel irradiated with 80 MeV Iodine ions to 1×10^{17} ions/cm^2 at the irradiation temperatures of 140 and 200 °C [13]. A thin amorphous layer of U-Mg at the U(Mo)/Mg interface was identified with a thickness of approximately 50 nm and

* Corresponding author. Nuclear Fuels and Materials Division, Idaho National Laboratory, P.O. Box 1625, Idaho Falls, ID 83415-6188, USA.
E-mail address: Jian.Gan@inl.gov (J. Gan).

http://dx.doi.org/10.1016/j.jnucmat.2017.07.030
0022-3115/Published by Elsevier B.V.

Table 1
Irradiation conditions of U-7Mo/Mg fuel samples for TEM characterization.

Sample I.D. (Fuel plate ID: R9R010)	KGT-1225 low flux	KGT-1222 high flux
Sample local fission density (10^{27} f·m^{-3})	3.7	5.5
Time-averaged local fission rate (10^{20} f·m^{-3}·s^{-1})	7.4	11.0
Fuel temperature at fuel plate middle plane at beginning of fuel life (°C)	119	145
Fuel temperature at fuel plate middle plane at end of fuel life (°C)	127	171
Time-averaged fuel middle plane Temperature (°C)	123	158

110 nm at 140 and 200 °C, respectively. The estimated atomic displacement damage near the U(Mo)/Mg interface region from nuclear stopping is greater than 50 displacements per atoms (dpa). The μ-XRD results show that, at low irradiation temperature of 140 °C, no irradiation-induced phase detected at U(Mo)/Mg interface region and, at high irradiation temperature of 200 °C, an irradiation-induced phase of $U_{0.9}Mg_{0.1}$ was detected with a bcc structure with a lattice constant of 0.3313 nm and nanoparticle size of ~16 nm. The general conclusion from Chiang's ion irradiation study of U(Mo)/Mg interface is that Mg may be used to replace Al matrix to suppress the amorphous FMI region.

Kammerer et al. investigated the reaction of pure Mg and Al alloy 6061 using diffusion couples heat treated at 300 °C for 720 h, 350 °C for 360 h and 400 °C for 240 h [14]. Microstructural characterization includes optical microscopy, SEM and TEM. The reaction product at Mg/Al 6061 interface include a thin $Al_{12}Mg_{17}$ (γ-phase) layer, a much thinner $Al_{30}Mg_{23}$ (ε-phase) layer and a thick Al_3Mg_2 (β-phase) layer although the ε-phase was not identified in the diffusion couple tested at 400 °C. They concluded that the activation energy for the growth of γ-$Al_{12}Mg_{17}$ was significantly higher than that for β-Al_3Mg_2 while the activation energy for interdiffusion of γ-$Al_{12}Mg_{17}$ was only slightly higher than that for β-Al_3Mg_2.

Huang et al. performed interdiffusion experiments using U-7Mo alloy and pure Mg at 550 °C for 96 h [15]. They used scanning electron microscopy (SEM) and transmission electron microscopy (TEM) to show that negligible interaction had occurred in the annealed diffusion couple.

Furthermore, researchers at the Canadian Nuclear Laboratory (CNL) are irradiating CNL-fabricated pin-type AA 1060-clad U-7Mo/Mg and U-10Mo/Mg mini-elements with a uranium loading of 4.5 gU/cm^3. The mini-elements are being irradiated in the Research Universal (NRU) reactor at a nominal power of 100 kW/m to a target burnup of 80 at. % U-235 depletion [16]. Structure and thermal property calculations have been completed to support the irradiation experiment [17], but detailed SEM or TEM characterization results have yet to be reported.

This paper reports the first microstructural characterization information from a neutron-irradiated U-7Mo/Mg matrix fuel using TEM. The TEM characterization was performed on samples taken from the low-flux and high-flux sides of the same fuel plate with U-7Mo fuel particles dispersed in Mg matrix with aluminum alloy Al6061 as cladding material. The corresponding local fission density and life-averaged fission rate of the fuel particles and the peak fuel-plate centerline temperature for the low-flux and high-flux samples are calculated to be 3.7 × 10^{21} f/cm^3, 7.4 × 10^{14} f/cm^3/s and 123 °C, and 5.5 × 10^{21} f/cm^3, 11.0 × 10^{14} f/cm^3/s and 158 °C, respectively. These TEM results, combined with the previously published SEM results, provide new insights on the irradiation performance of the U(Mo) fuel with Mg matrix, which appears to be a viable alternative to Al-based alloys as the matrix for U(Mo) dispersion fuels.

2. Experiment

The R9R010 dispersion fuel plate (U-7Mo/Mg, 58.2% enrichment) was irradiated in the ATR for approximately 90 effective full power days. The fuel plate was positioned edge-on with respect to the reactor core. As a result of steep neutron flux gradient across the width of the fuel plate, one side was irradiated under the relatively low flux while the other side was irradiated under high flux. Table 1 summarizes the irradiation conditions of the TEM samples. Small cylindrical punchings of 1.0 mm in diameter and roughly 1.4 mm in length were produced from both the low-flux and the high-flux sides of the fuel plate at the Hot Fuel Examination Facility (HFEF) at INL. SEM Met-Mount samples were prepared in a glove box at the Electron Microscopy Laboratory (EML). SEM analysis with both secondary electron (SE) and backscattered electron (BSE) images were produced from the polished samples. Compositional analysis was performed using energy-dispersive spectroscopy (EDS) and wavelength-dispersive spectroscopy (WDS). TEM lamella samples were produced from the SEM samples using an FEI Quanta3D Dual-Beam focused ion beam (FIB) system. Multiple "lift-outs" were produced at specific sites of the SEM samples as shown in Figs. 1

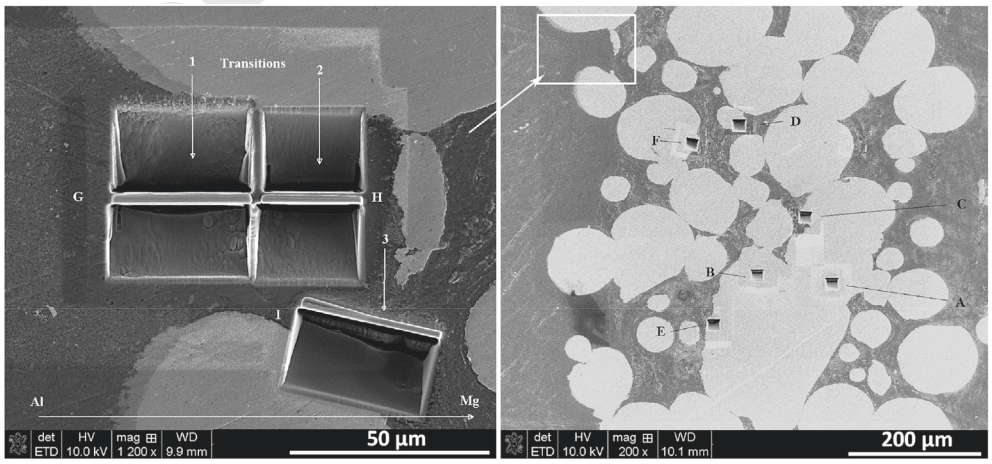

Fig. 1. SEM images of TEM lamella site map (right) and a magnified view (left) of the boxed area for low fission density sample (3.7 × 10^{21} f/cm^3) with labels showing where the lamella were lift-out.

Please cite this article in press as: J. Gan, et al., TEM characterization of irradiated U-7Mo/Mg dispersion fuel, Journal of Nuclear Materials (2017), http://dx.doi.org/10.1016/j.jnucmat.2017.07.030

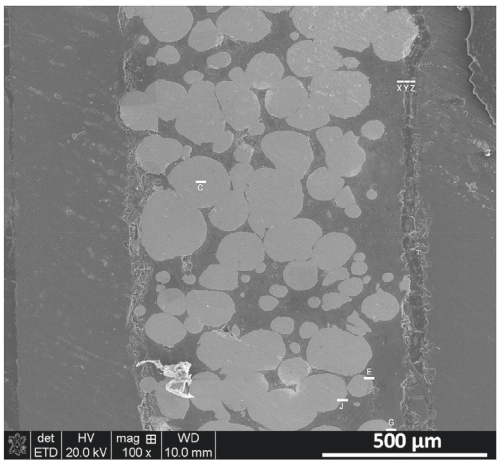

Fig. 2. SEM image of TEM lamella site map for high fission density sample (5.5×10^{21} f/cm^3) with labels showing where the lamellas were lift-out.

Table 2
List of site specific TEM lamellas prepared by FIB lift-out.

TEM Lamella site ID:	Note
Low fission density	KGT-1225
D, F	U(Mo)/Mg interface
A, B	U(Mo) fuel particle interior
G, H, I	Al cladding to Mg matrix interface
	Areas C & E only for SEM
High fission density	KGT-1222
G, J, E	U(Mo)/Mg interface
C	U(Mo) fuel particle interior
X, Y, Z	Al cladding to Mg matrix interface

and 2 for low fission density (KGT-1225) and high fission density (KGT-1222), respectively. A list of TEM lamellas for both low flux and high flux samples are shown in Table 2. TEM characterization was carried out using a 200-kV JEOL-2010 TEM equipped with a 16-bit digital camera (2048 × 2048 pixels) and a silicon drift detector (SDD) for composition analysis with EDS. Both TEM and scanning-TEM (STEM) imaging were used to capture various microstructural features. Selected area diffraction (SAD) was used to identify the structural information of interaction product and various precipitates. Composition analysis was carried out using EDS in STEM in spot mode, line scan and 2D elemental mapping.

3. Results and discussion

The TEM characterization results are presented in the following three sections: 1) U(Mo) fuel particle interior, 2) U(Mo)/Mg interface and 3) Mg/Al 6061 interface. Both low and high fission density conditions are compared to reveal the microstructural evolution as a function of fission density. Some cross comparisons of TEM and SEM results have been made to better describe the irradiated microstructure at different scales and the associated interaction phases at the interfaces. The results from this TEM work are discussed in the context of those reported in the literature for an ion irradiation study of U(Mo)/Mg fuel and the thermal annealing study of the Mg/Al-6061 diffusion couples [13,14].

It is well known that TEM and SEM are complementary microstructural characterization techniques. TEM is capable of revealing microstructural details at near-atomic resolution and of analyzing defects and precipitates through diffraction or absorption contrasts and microchemistry analysis. In contrast, the large bubbles of several µm in sizes, as well as the general microstructure shown in the SEM images in Figs. 1 and 2, cannot be captured in the TEM images because their sizes are beyond the limit for TEM analysis. Unlike irradiated structural materials which are relatively uniform in general, the microstructure of the irradiated fuel at high fission density can be highly heterogeneous on the µm scale. It is a general practice to characterize irradiated fuel samples using optical microscopy, SEM and TEM to capture the major microstructural features over a broad length scale. It is recognized that, while site-specific TEM lamella from FIB lift-out allows one to reveal local microstructures that typically cannot be revealed using conventional TEM sample preparation techniques, the overall sample areas for TEM analysis of FIB lamellas are quite limited due to their small size (~15 × 15 µm^2). It is always challenging to draw a general conclusions based on just the TEM analysis of a limited number of relatively small TEM lamellas that are made from the highly heterogeneous microstructure of an irradiated fuel. Due to the challenges of working with highly-irradiated fuel samples, typically only a small number of TEM samples can be characterized. Nevertheless, the information acquired through TEM analysis is extremely important to help improve the understanding of the microstructural behavior of the fuels under irradiation and the impact of changes in microstructure and microchemistry on the fuel performance.

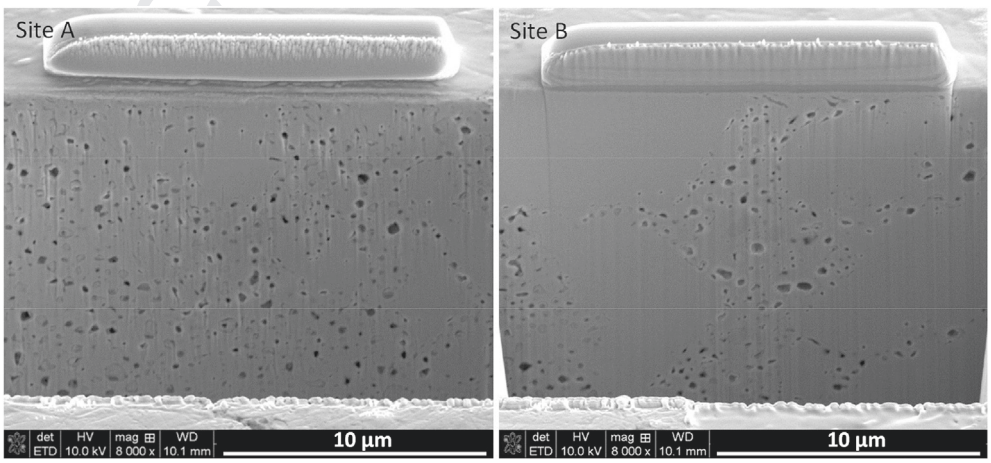

Fig. 3. Comparison of SEM overview images of site A (left) and site B (right) for the interior of two different U(Mo) fuel particles at local fission density of 3.7×10^{21} f/cm^3.

Please cite this article in press as: J. Gan, et al., TEM characterization of irradiated U-7Mo/Mg dispersion fuel, Journal of Nuclear Materials (2017), http://dx.doi.org/10.1016/j.jnucmat.2017.07.030

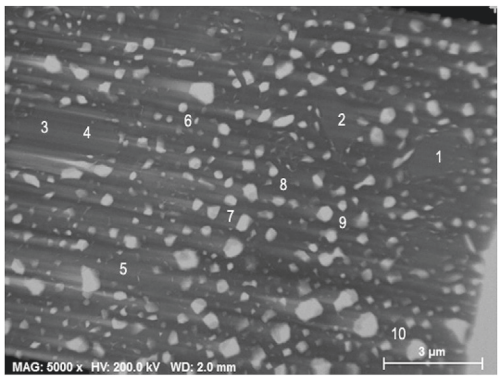

Fig. 4. Low magnification STEM image of site A lamella with labels for EDS measurements.

Table 3
EDS measurement from area labeled in Fig. 3.

Spot	U (wt%)	Mo (wt%)	Note
1	89.2	10.8	Relatively clean area
2	89.1	10.9	Relatively clean area
3	88.9	11.1	Relatively clean area
4	89.7	10.3	Relatively clean area
mean	89.2	10.8	
5	90.7	9.3	Area surrounded by bubbles
6	89.9	10.1	Area surrounded by bubbles
7	90.6	9.4	Area surrounded by bubbles
8	90.5	9.5	Area surrounded by bubbles
9	92.7	7.3	Area surrounded by bubbles
10	90.4	9.6	Area surrounded by bubbles
mean	90.8	9.2	

3.1. Microstructure of U(Mo) fuel particle interior

At a local fission density of 3.7 × 10^{21} f/cm^3, a comparison of SEM images of the sectional view for sample from site A and B is shown in Fig. 3. It clearly shows the heterogeneous microstructure of the irradiated U(Mo) fuel where site A shows noticeably higher volume fraction of bubbles than that of site B under the same nominal fission density. One possible cause of the higher number density of bubbles seen in site A is that smaller grains in that region promote the development of more large grain boundary bubbles due to the presence of more grain boundaries.

A low magnification STEM image of site A with areas labeled for EDS measurement in spot mode is shown in Fig. 4. Most of these

Table 4
EDS measurement from area labeled in Fig. 4.

Spot	Sr	Y	Zr	Mo	Ba	Ce	Nd	U
1	37.6	18.0	16.4	1.2	19.0	6.2	0.2	1.5
2	28.4	25.5	30.5	1.9	0	12.5	0	1.2
3	24.7	15.3	18.4	7.1	4.1	12.0	7.5	10.9
4	18.8	27.0	32.9	0	10.3	11.0	0	0
5	23.2	25.2	18.5	4.2	15.5	10.3	0.9	2.1
6	21.5	28.0	20.7	1.9	6.2	20.0	0	1.7
mean	25.7	23.2	22.9	2.7	9.2	12.0	1.4	2.9

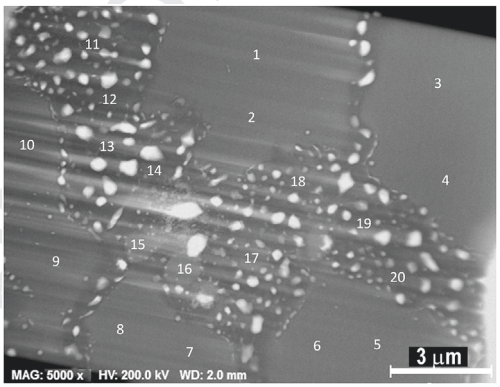

Fig. 6. Low magnification STEM image of site B with area labeled for EDS measurement.

bubbles are faceted with a broad size range from ~1 μm down to ~50 nm. Some elongated bubbles are clearly visible, indicating bubble coarsening likely occurred at the specified fission density at grain boundary regions. Since the EDS measurements reveal that the summation of the U and Mo composition is approximately 95 wt.%, for simplicity on the effect of local Mo concentration on bubble morphology and distribution, only the results of EDS measurement on U and Mo is tabulated in Table 3. Looking at the results for spots 1–4 that are from relatively clean areas and spots 6–10 that are more closely surrounded by bubbles, a rough estimate shows that the average Mo concentrations in the relatively clean area vs. the area closely surrounded by bubbles is 10.8 wt% and 9.2 wt%, respectively. This difference is generally consistent with the role of Mo on stabilizing the bcc phase in U(Mo) for better microstructural behavior under irradiation. Note that Mo is also a fission product with high fission yield therefore the irradiated U(Mo) fuel is expected to have higher Mo than its nominal 7.0 wt%

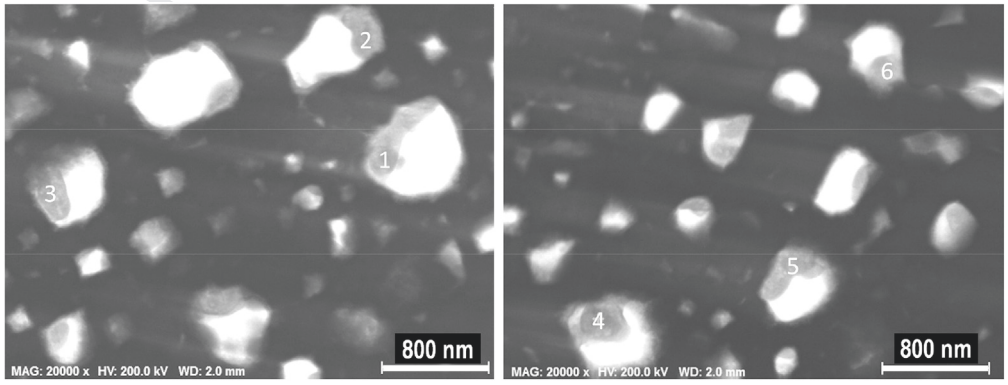

Fig. 5. Intermediate magnification STEM image of site A with labels for EDS measurement on solid fission product accumulated inside the large bubbles.

Please cite this article in press as: J. Gan, et al., TEM characterization of irradiated U-7Mo/Mg dispersion fuel, Journal of Nuclear Materials (2017), http://dx.doi.org/10.1016/j.jnucmat.2017.07.030

Table 5
EDS measurement in wt.% from area labeled in Fig. 6.

82. Spot	U	Mo	Note	Spot	U	Mo	Note
1	86.9	13.1	Clean area	11	91.6	8.4	Bubble area
2	88.5	11.5		12	92.1	7.9	
3	89.0	11.0		13	91.7	8.3	
4	88.1	11.9		14	91.0	9.0	
5	88.5	11.5		15	97.5	2.5	
6	88.5	11.5		16	97.0	3.0	
7	89.0	11.0		17	90.9	9.1	
8	88.2	11.8		18	92.3	7.7	
9	87.3	12.7		19	91.7	8.3	
10	88.7	11.3		20	91.5	8.5	
mean	88.3	11.7	Clean area	mean	92.7	7.3	Bubble area

in the fresh fuel. The fluctuation in local Mo content in the irradiated fuel particles could also be attributed to the heterogeneous distribution of Mo and U-235 in the U(Mo) fuel feedstock that was used to produce the atomized U(Mo) fuel particles for dispersion fuel.

The STEM image of the same area at higher magnification is shown in Fig. 5. Solid fission product accumulation at these large bubbles is evident. EDS measurements of the features labeled in the STEM image are listed in Table 4. The average composition over the 6 EDS measurements in atomic percentage is approximately 26%Sr, 23%Y, 23%Zr, 3%Mo, 9%Ba, 12%Ce, 1%Nd and 3%U. The precipitation of solid fission product (SFP) to the large bubbles has been observed in previous work [18]. Although Mo is also a high yield fission product like Zr, but its content is quite low in these SFP precipitates, likely contained in the U(Mo) fuel matrix. Note that this SFP precipitation at large bubbles in irradiated U(Mo) is similar to the 5-metal precipitates (Pd-Rh-Ru-Tc-Mo) observed in the irradiated UO_2 [19], although there are large difference in fuel material (metal vs. oxide), irradiation temperature (low vs. high) and fission density (high vs. low) among the two fuels.

As shown in Fig. 3, the microstructure of sample site B is quite different from that of site A. A low magnification STEM image of site B is shown in Fig. 6. The labels indicate where EDS measurements for U and Mo were performed. Spots 1–10 are in the clean areas without large bubbles while spots 11–20 are located in the areas surrounded by bubbles in a “thick band”. The EDS composition results are listed in Table 5. Note that Mo depletion at the grain boundary region is typically observed for U(Mo) fuel, which may

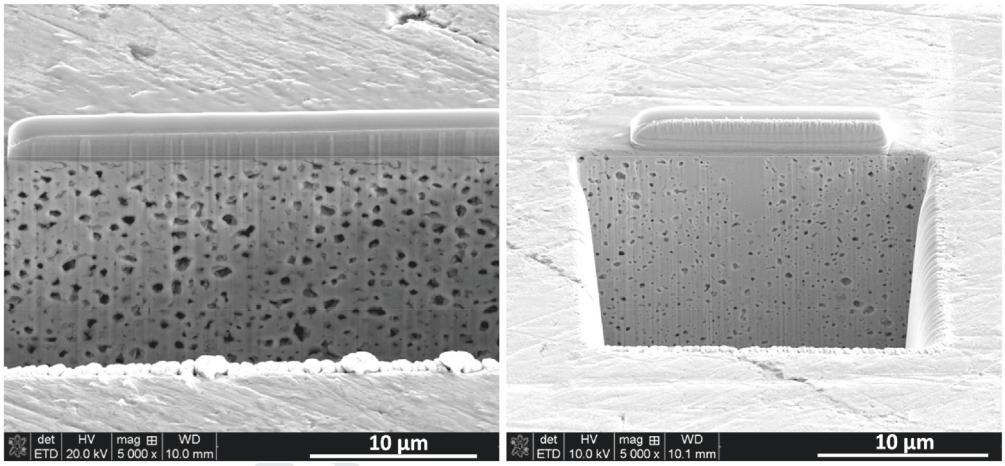

Fig. 7. Comparison of SEM sectional view of U(Mo) fuel from site C of high fission density (left) (5.5×10^{21} f/cm^3) and site A of low fission density (right) (3.7×10^{21} f/cm^3).

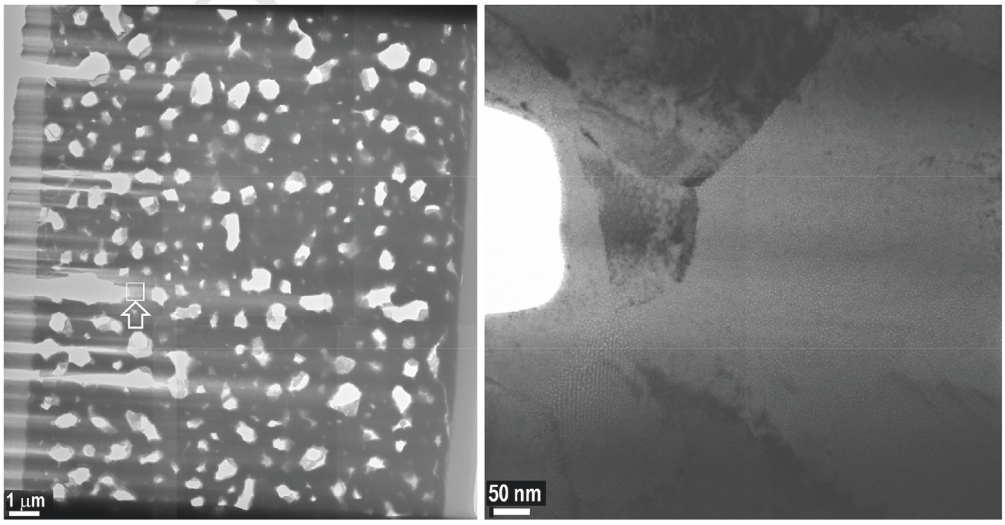

Fig. 8. A montage (left) of TEM low magnification image of irradiated U(Mo) from site-C at a high fission density (5.5×10^{21} f/cm^3) and a high magnification view (right) of the small boxed area showing the subdivided grains with small pocket of residual GBS in the low-left corner.

Please cite this article in press as: J. Gan, et al., TEM characterization of irradiated U-7Mo/Mg dispersion fuel, Journal of Nuclear Materials (2017), http://dx.doi.org/10.1016/j.jnucmat.2017.07.030

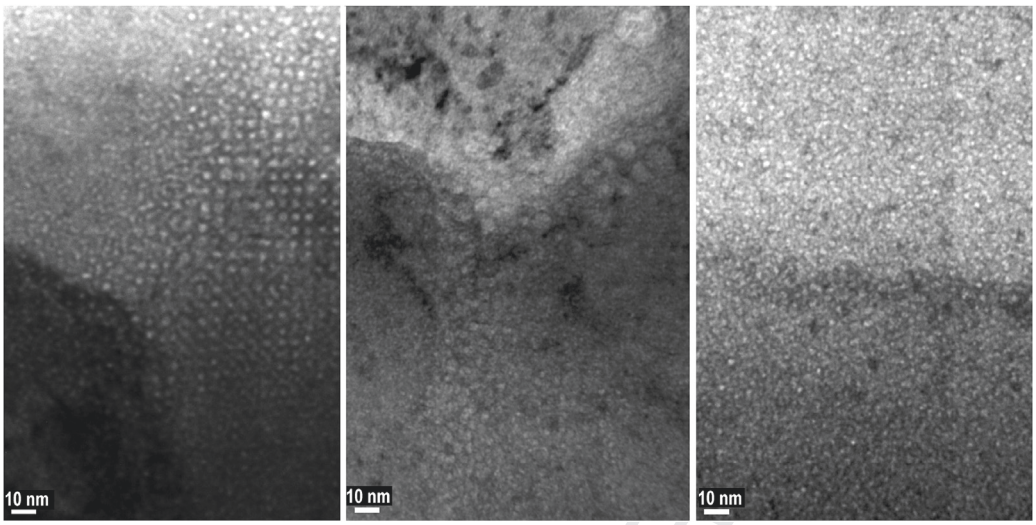

Fig. 9. TEM high magnification images of irradiated U(Mo) from site-C reveal various features of small pocket of GBS oriented at [100] zone (left), bubble coarsening (middle) and random distribution of fine bubbles (right) at a fission density of 5.5×10^{21} f/cm^3.

help promote early development of large bubbles in these regions. This is due to the possible presence of a less stable γ-phase (bcc) in U(Mo) due to the lower Mo content compared to the target concentration of 7 wt.% Mo for the fuel that can potentially result in poorer irradiation performance [2]. The EDS data show a significant difference in Mo content between the clean area (11.7 ± 0.7 wt.%) and bubble area (7.3 ± 2.4 wt.%). Spot 15 and 16 may be on an α-U phase based on the very low Mo content. By excluding these two data points, the average Mo content from the bubble area will change to 8.4 wt%, which is still 28% lower than 11.7 wt% from the clean area. Note that the clean areas shown for both site A and B are filled with very high concentrations of fine fission gas bubbles of ~3 nm arranged in an fcc gas bubble superlattice (GBS) which were investigated extensively in the previous work [20,21]. Since the TEM lamella produced from site A and B are not thin enough for detailed TEM characterization, the high magnification TEM images of GBS are not available for these two sample conditions.

At a high fission density of 5.5×10^{21} f/cm^3, the average size of

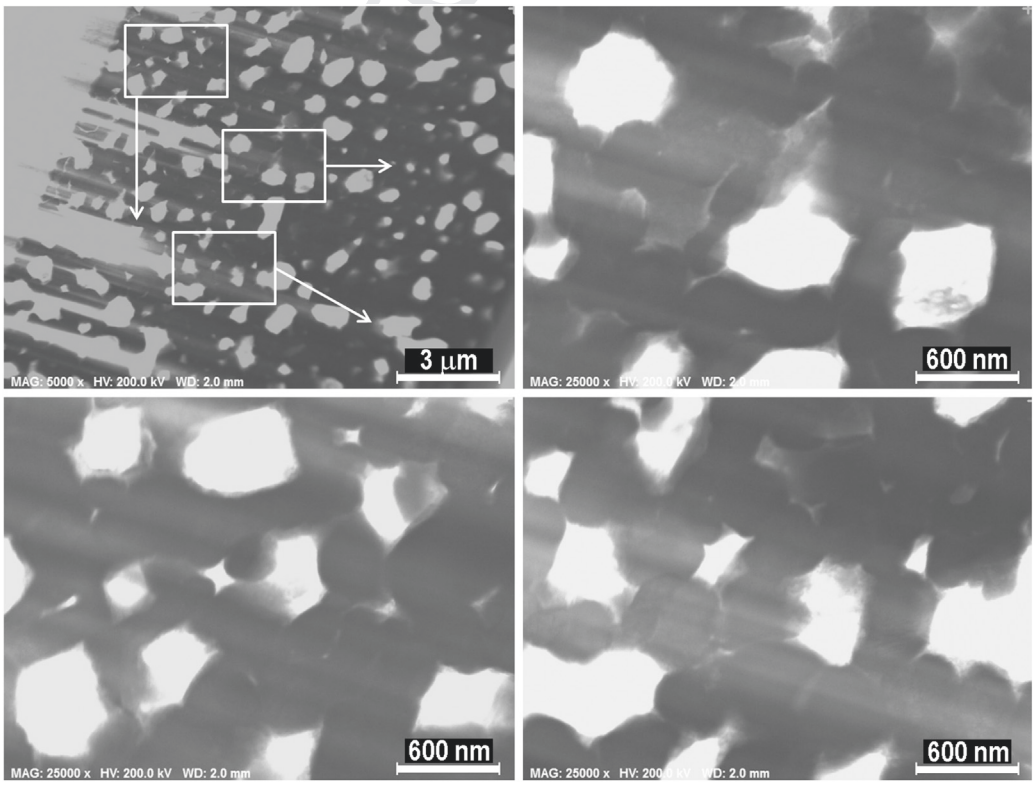

Fig. 10. STEM images of low magnification (upper-left) and the detailed microstructure of the boxed area showing large bubbles surrounded by U(Mo) fragments consisting of subdivided grains from site-C for the high fission density sample (5.5×10^{21} f/cm^3).

Please cite this article in press as: J. Gan, et al., TEM characterization of irradiated U-7Mo/Mg dispersion fuel, Journal of Nuclear Materials (2017), http://dx.doi.org/10.1016/j.jnucmat.2017.07.030

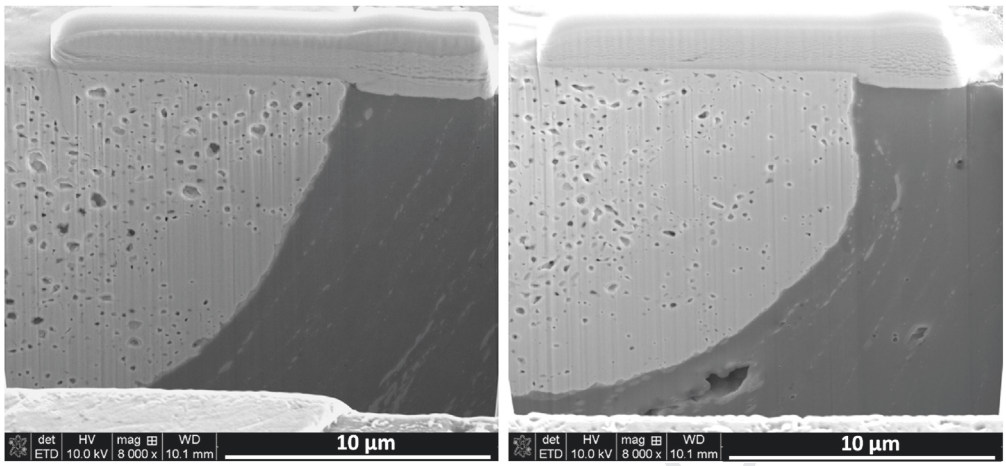

Fig. 11. SEM low magnification images of sectional view of site F (left) and site D (right) from low fission density sample (3.7×10^{21} f/cm^3).

the large bubbles is significantly larger than for the low fission density (3.7×10^{21} f/cm^3) sample, as shown in Fig. 7, which compares the SEM images for the sectional view from site C of KGT-1222 and for site B of KGT-1225. Fig. 8 shows a montage (left) of TEM low magnification images of irradiated U(Mo) from site-C and a high magnification view (right) of the small boxed area showing the subdivided grains with small pockets of residual GBS in the low-left corner. Note that there is no evidence of large bubble development

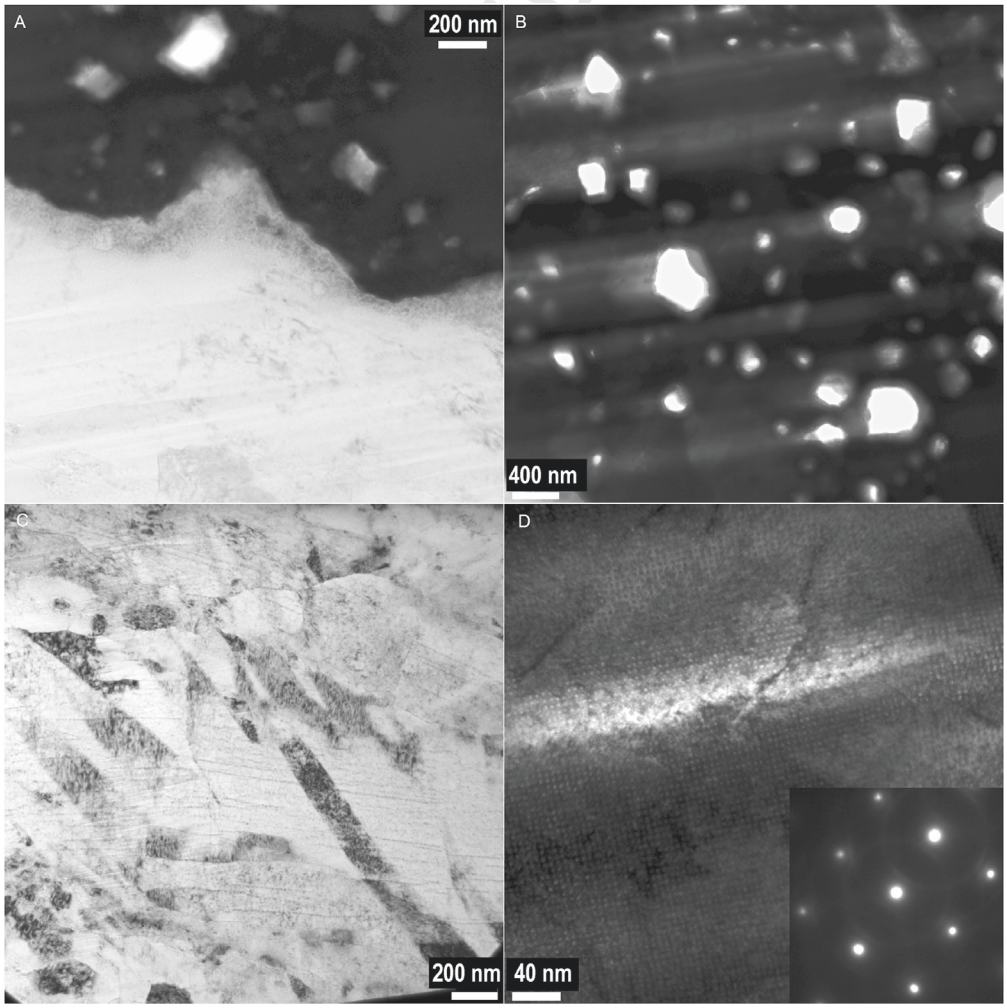

Fig. 12. TEM images of site F at 3.7×10^{21} f/cm^3 at low magnification reveal U(Mo)/Mg interface (A), U(Mo) fuel particle interior (B), Mg matrix (C), and high magnification view of GBS fine bubbles at zone [100] of U(Mo) (D) where the inset shows the select area diffraction at zone [100] of U(Mo).

Please cite this article in press as: J. Gan, et al., TEM characterization of irradiated U-7Mo/Mg dispersion fuel, Journal of Nuclear Materials (2017), http://dx.doi.org/10.1016/j.jnucmat.2017.07.030

at the boundaries of subdivided grains. Fig. 9 shows the TEM bright field images of detailed microstructural features from different region of the irradiated U(Mo) at high magnification. The image on the left reveals the pocket of residual GBS oriented at zone [100] in bcc U(Mo). The image in the middle captures bubble coarsening similar to what was reported in the previous work [18]. The image on the right displays the random distribution of fine bubbles at very high number density (see Fig. 10).

3.2. Microstructure at U(Mo) fuel and Mg matrix interface

The irradiated microstructure at the interface of U(Mo) fuel particle and Mg matrix was of particular interest for this TEM investigation, since finding a material that does not interact with U-7Mo would be very beneficial. For dispersion fuel with Al or Al alloy matrix, U-7Mo fuel can react with the matrix during fuel fabrication to form fuel-matrix interaction (FMI) intermetallic phases, and this interaction will continue during reactor irradiation. It is desirable to suppress FMI by physical means, where one of the approaches is to use an alternative material like Mg, which is a material that will not react with U-7Mo during irradiation. It is of interest to see if there actually is FMI at a very fine scale. TEM is required to make this determination.

At fission density of 3.7×10^{21} f/cm^3, SEM images of the sectional view for samples from site F and D are shown in Fig. 11. Both images show no evidence of contrast variations that may indicate the presence of an interaction product at the interface. Unlike that of Al alloy matrix U(Mo) dispersion fuel where large bubbles tend to develop near the FMI/matrix interface, it appears that the population of large bubbles in U(Mo) fuel for the Mg matrix dispersion fuel is into the U-7Mo fuel particle away from the fuel-matrix interface. This may be explained by the lack of FMI layer in Mg matrix fuel, which is speculated to improve the heat conduction at the interface, therefore keeping the local temperature low and suppressing the mobility of fission gas atoms. Note that even with a fuel fabrication defect shown in Mg matrix as a relatively large cavity for site D sample, there is no evidence of negative impact on the irradiated microstructure in U(Mo) in term of large bubbles, likely attributed to the good thermal conductivity at the U(Mo) fuel and Mg matrix interface. Defects in the Mg matrix in the fresh fuel can be reduced through optimization of fuel fabrication processing. This particular fuel plate was a test plate where the fabrication methods were not optimized.

TEM images of site F at low magnification for interface region and high magnification for the GBS fine bubbles oriented at zone [100] of bcc U(Mo) are shown in Fig. 12. At the U(Mo)-Mg matrix interface, a thin layer of <200 nm contrast variation from Mg matrix is observed (Fig. 12 A). The interior of U(Mo) fuel particle consists of areas with and without large bubbles (Fig. 12 B), similar to that shown in Fig. 4. The TEM image of Mg matrix at low magnification reveals some elongated grain texture (Fig. 12 C). Mg remains crystalline and no fission product was detected by EDS. A high magnification TEM bright field image (Fig. 12 D) from the clean area of U(Mo) oriented at zone [100] shows GBS fine bubbles. It is well known that this GBS has a fcc super structure with all three major axes coincident with bcc U(Mo). The measurement on the GBS indicates an average bubble size of 3.5 ± 0.2 nm and a superlattice constant of 11.2 nm, consistent with the previous measurements for GBS [20,21].

The composition analysis of the fuel-matrix interface region is shown in Fig. 13 with labels for EDS measurement in spot mode, along with three EDS spectrum collected from three distinctively

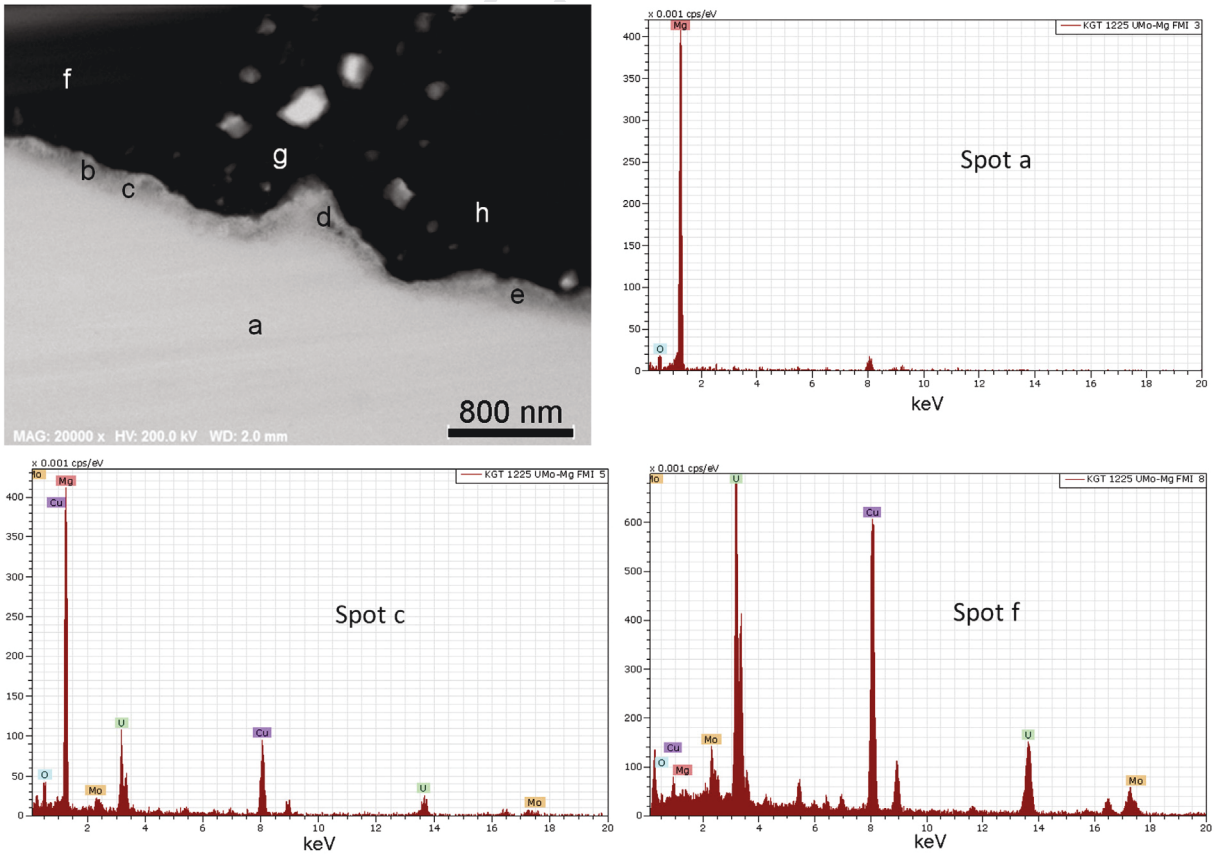

Fig. 13. STEM image with labels for EDS measurement and the EDS spectrum from spot a, c and f for site F at low fission density of 3.7×10^{21} f/cm^3.

Please cite this article in press as: J. Gan, et al., TEM characterization of irradiated U-7Mo/Mg dispersion fuel, Journal of Nuclear Materials (2017), http://dx.doi.org/10.1016/j.jnucmat.2017.07.030

Table 6
EDS result of U(Mo)/Mg interface in wt.% from areas labeled in Fig. 13.

Spot	Mg	U	Mo	Note
a	94.7	3.0	2.3	Mg matrix
a2	96.9	2.2	0.9	Mg matrix
b	20.0	70.8	9.2	Mg side next to U(Mo), ~68 at.% Mg
c	48.5	45.1	6.4	Mg side next to U(Mo), ~89 at.% Mg
d	35.5	57.4	7.1	Mg side next to U(Mo), ~82 at.% Mg
e	31.7	60.3	8.0	Mg side next to U(Mo), ~79 at.% Mg
f	0	90.3	9.7	U(Mo) near interface
g	0.2	93.4	6.4	U(Mo) near interface
h	0	90.2	9.8	U(Mo) near interface

different region. Note that the Cu peaks are the result of the Cu grid used for TEM lamella, which is enhanced when X-rays from heavier elements are excited. These peaks are typically ignored for quantitative analysis. The results of EDS measurements in wt.% are listed in Table 6. The narrow region of contrast variation at the U-7Mo/Mg interface is of interest, and the composition measurements that were taken had an average Mg concentration of ~34 wt.% or ~80 at.% Mg as a mean of the EDS measurements for spots b, c, d and e in Table 6. It appears that small amounts of U and Mo accumulate in this narrow band of less than 200 nm where no convincible evidence of fission gas bubbles can be found. One possible mechanism is radiation enhanced mixing at the interface. Due to the lack of diffusion reaction between U(Mo) and Mg, the width of mixing at

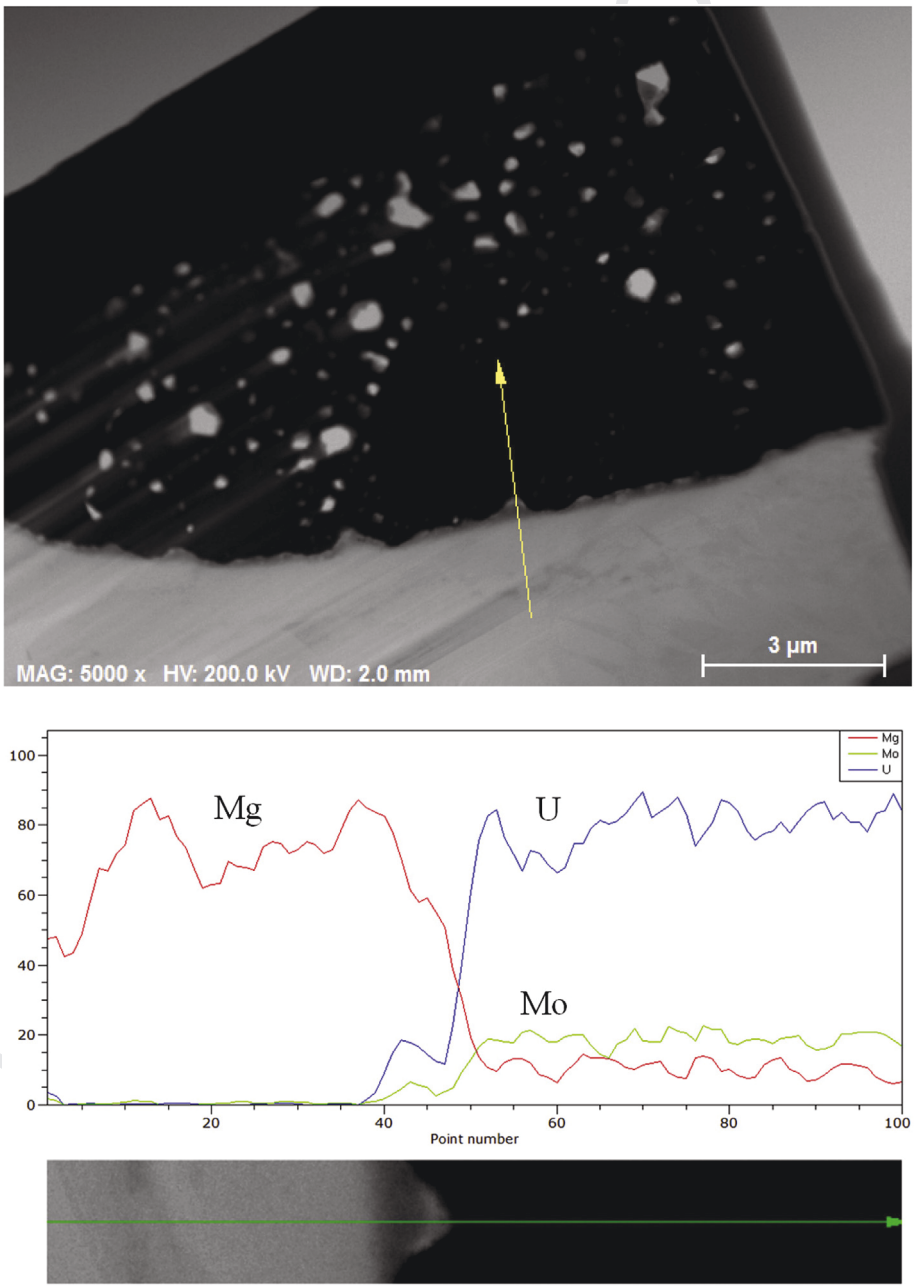

Fig. 14. Low magnification STEM image and EDS line scan in arbitrary unit of x-ray intensity at U(Mo)/Mg interface for site F of low fission density sample (3.7×10^{21} f/cm^3).

Please cite this article in press as: J. Gan, et al., TEM characterization of irradiated U-7Mo/Mg dispersion fuel, Journal of Nuclear Materials (2017), http://dx.doi.org/10.1016/j.jnucmat.2017.07.030

the interface is very limited. Inside the U(Mo) fuel interior, the measured U and Mo for site F is in agreement with the result shown in Table 3 for site A at the low fission density.

Fig. 14 shows low magnification STEM image and EDS line scan in arbitrary unit of X-ray intensity at the U(Mo)/Mg interface for site F. There are one hundred data points for the specified line scan. The composition profile could be linked to the elemental X-ray intensity profile. It clearly reveals a slightly increase in U and Mo in the narrow band of contrast variation in Mg near the interface. This narrow band is seen around the interface with varying width.

At high fission density of 5.5×10^{21} f/cm^3, SEM images with sectional views of the U(Mo)/Mg interface from site G, J and E are shown in Fig. 15. The microstructure at the interface looks similar to that at low fission density. The high magnification view for site G reveals some U(Mo) debris at the interface. This debris is likely resulted from fuel fabrication since it is only observed in few spots at the interface. The lack of large bubbles in U(Mo) near the interface region is evident even at high fission density, which is consistent with the observation at low fission density. Fig. 16 shows STEM low magnification image along with an EDS line scan across the U(Mo)/Mg interface as well as the debris and several features in Mg matrix with varying contrast. The composition profile and EDS measurement confirm the black debris as U(Mo) and the dark gray feature as Mg-O compound. Fig. 17 shows the TEM images revealing the details of the interface at high magnification for area with debris-like features shown on the left and the area with a narrow band along the interface shown on the right with slightly dark contrast than the Mg matrix. EDS analysis shows the composition of this narrow band in at.%, which is approximately 83% Mg, 11% U and 6% Mo. This is in general agreement with the EDS measurement at the low fission density where the value was ~80 at% Mg. Based on the shape of these small features, these could be the result of precipitation of U(Mo) from the mixing of U(Mo) and Mg at the interface caused by energetic fission fragments. The width of the narrow band appears similar to that of low fission density although small particulate features are more evident at the high fission density. At high fission density, the Mg matrix still remains crystalline while MgO turns to amorphous. It suggests the oxygen contamination during the fuel fabrication process could have a direct impact to its irradiated microstructure. Fission product accumulation in Mg matrix was not detected by EDS.

In comparison to the ion irradiation study, Chiang et al. reported that the radiation induced phase of $U_{0.9}Mg_{0.1}$ was found at 200 °C, but not at 140 °C. This radiation-induced phase was not identified in the neutron-irradiated Mg matrix dispersion fuel at the interface region from this work. The time averaged fuel centerline temperature for low and high fission density sample are calculated to be 123 °C and 158 °C, respectively [12]. The irradiation temperature between the ion and neutron irradiation seems comparable. In the ion irradiation with 80 MeV iodine ions, the total ion fluence was estimated to be equivalent to ~2.0×10^{20} f/cm^3 after ~17 h of irradiation, approximately 10% of the FRM II fuel element peak fission density [22]. This is more than one order of magnitude lower than the fission densities in this work. It is speculated that either

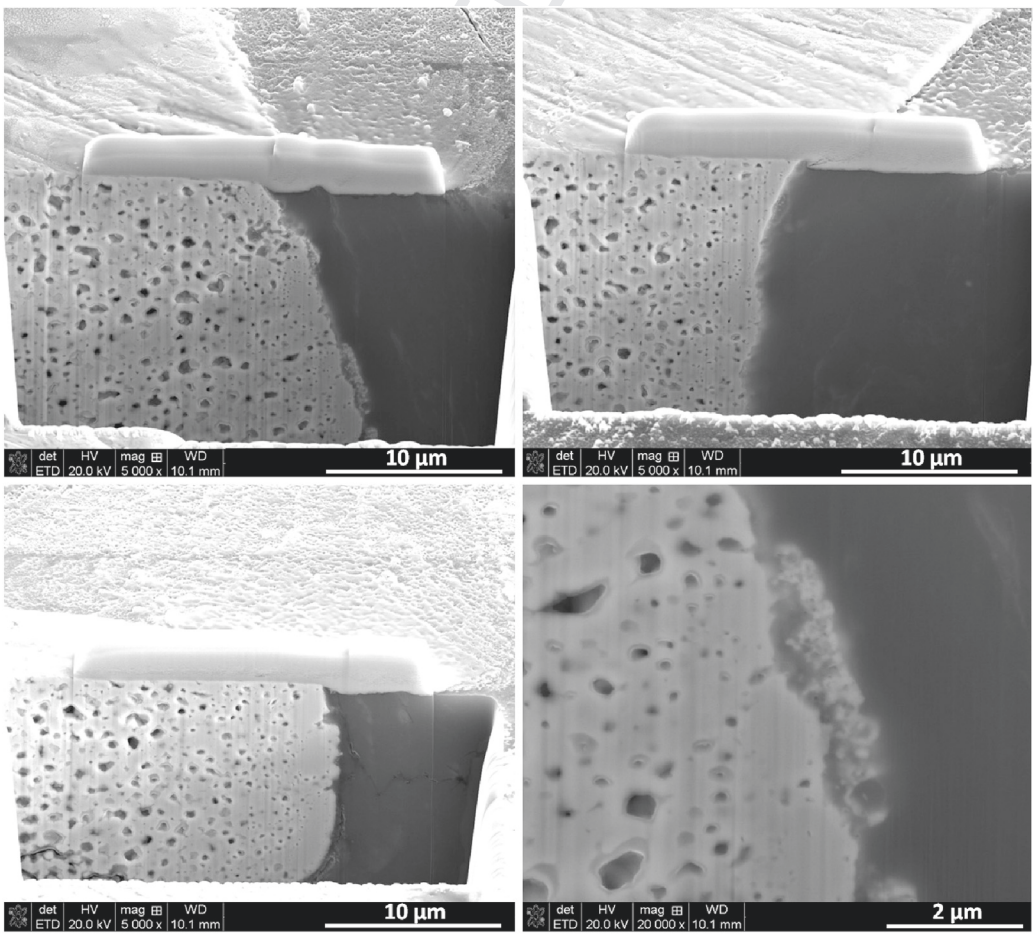

Fig. 15. Low magnification SEM sectional views of U(Mo)/Mg interface region at high fission density (5.5×10^{21} f/cm^3) for site G (top-left), site J (top-right) and site E (bottom left) and a high magnification image for site G (bottom right) from high fission density sample.

Please cite this article in press as: J. Gan, et al., TEM characterization of irradiated U-7Mo/Mg dispersion fuel, Journal of Nuclear Materials (2017), http://dx.doi.org/10.1016/j.jnucmat.2017.07.030

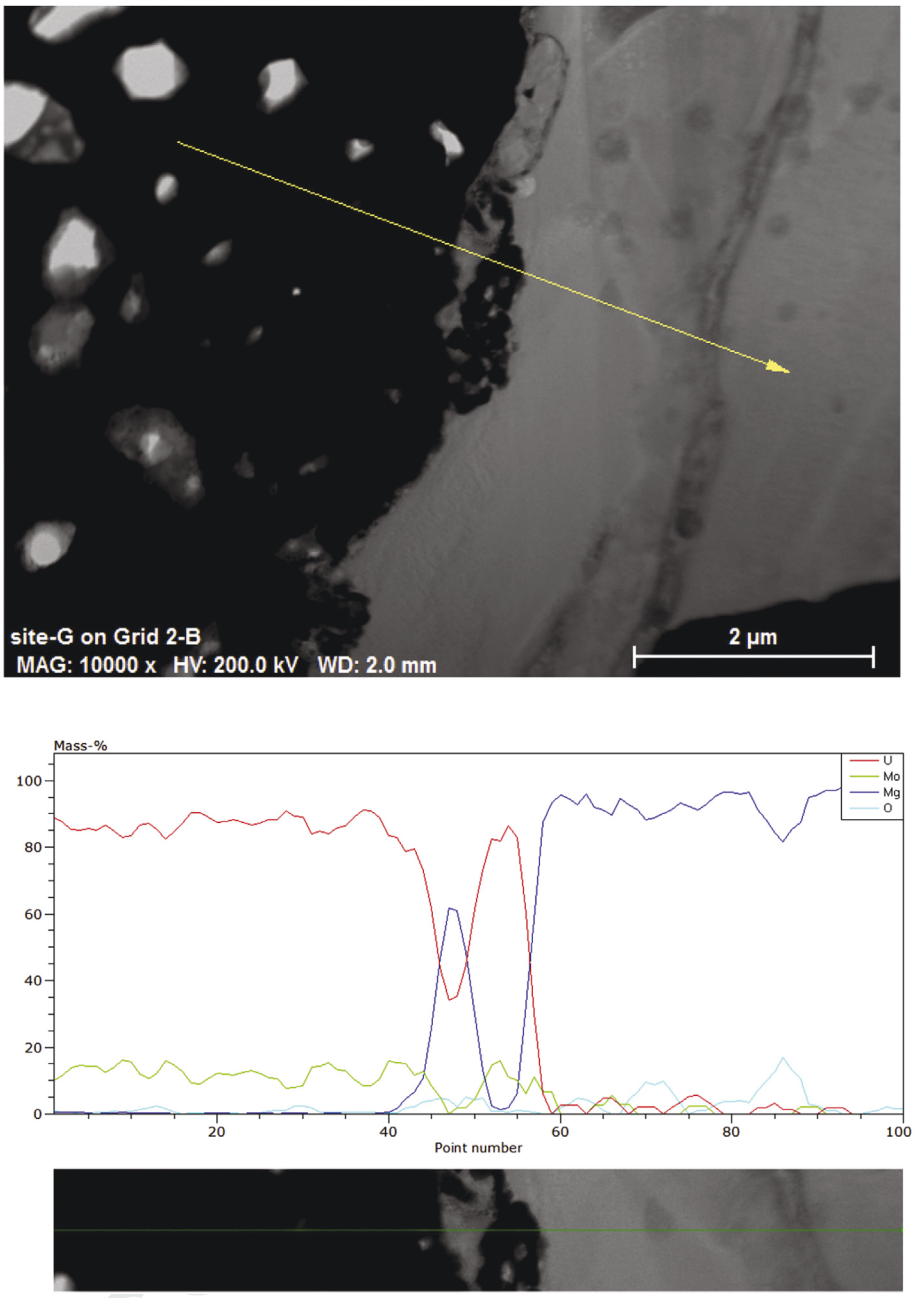

Fig. 16. STEM image of U(Mo)/Mg interface region at high fission density (5.5×10^{21} f/cm^3) for site TEM lamella along with EDS line scan of composition profile in wt.% where the black debris identified as U(Mo) and dark gray feature as Mg-O compound.

the radiation induced $U_{0.9}Mg_{0.1}$ phase could not form under the given neutron irradiation condition or this phase may only develop at low fission density and may dissolve at high fission density. Chiang also reported a thin amorphous layer of U-Mg with a thickness of 50 nm and 110 nm at 140 °C and 200 °C, respectively. This thin layer induced by ion irradiation appears similar to the narrow band seen in the neutron irradiated Mg matrix fuel at the U(Mo)/Mg interface except the latter is not amorphous. Based on the fluence and damage profile for ion irradiation and fission density for neutron irradiation, the estimated energy deposition rate in U(Mo) between the 80 MeV iodine ion irradiation and neutron irradiated high flux sample (KGT-1222) is 0.76×10^{21} and 0.42×10^{21} MeV/cm^3-hr, respectively. The higher energy deposition rate at relatively low irradiation temperature may result in the formation of the amorphous thin layer under ion irradiation.

3.3. Microstructure at Mg matrix - Al alloy cladding interface

The irradiated microstructure at the interface between Mg matrix and Al alloy cladding is also investigated in this work. Of interest in this region are the phases that are present after irradiation and the radiation stability of these phases. Since the TEM characterization of the fresh fuel condition is not available for comparison with the irradiated fuel, the microstructural features found at this interface may not be induced by irradiation. It is known that Mg typically reacts with Al at higher temperatures to form various interaction products as a result of diffusion reaction from fuel fabrication processes. The comparison of interface

Please cite this article in press as: J. Gan, et al., TEM characterization of irradiated U-7Mo/Mg dispersion fuel, Journal of Nuclear Materials (2017), http://dx.doi.org/10.1016/j.jnucmat.2017.07.030

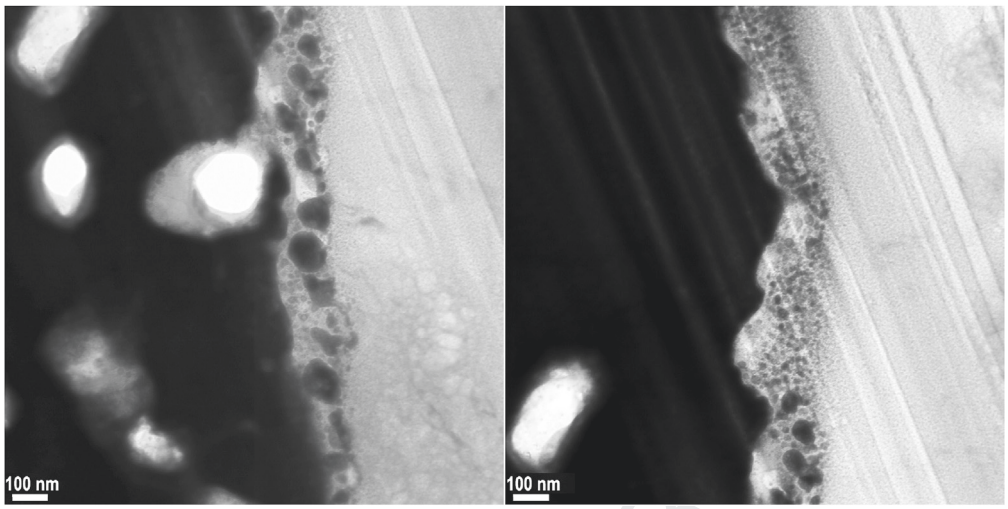

Fig. 17. TEM images of site F at high magnification with detailed view at interface region at high fission density (3.7×10^{21} f/cm^3) from two different areas where the image on the left showing more large particulate features than the image on the right.

microstructural features between the irradiated fuel and that of diffusion couple annealing experiment should be helpful to shed the light on the radiation stability of the reaction product at the interface and its potential impact on fuel performance.

FIB SEM low magnification images of sectional view of site G (left) and site H (right) at the interface of Mg matrix and Al cladding from a low fission density sample (3.7×10^{21} f/cm^3) are shown in Fig. 18. The left side of site G, as shown in the image, was cut from the Al alloy cladding, and the right side of site H was machined from the Mg matrix. Site I, which is partially visible in the low-right corner of the SEM image for site H, is further into the Mg matrix as shown in the FIB site map in Fig. 1. Note the large differences in the thickness of reaction product shown in Fig. 1 (left), where approximately 5 μm of interaction product is found at the U(Mo)-Al interface and negligible interaction product is observed at the U(Mo)-Mg interface. This local, relatively thick FMI layer is the result of direct contact of a U(Mo) particle with the Al alloy cladding at the interface of Mg matrix and Al alloy cladding. Complex microstructural features can be found in the SEM image of site G where various sizes of black and white precipitates are present. Site H is relatively clean in terms of large precipitates except for the presence of light gray features.

TEM images of site G shown in Fig. 19 (A–D) reveal more details on the transitional microstructure from Al alloy (cF4 structure) to Al_3Mg_2 (cF1832 structure) where the red arrows in low magnification image A identify the boundary between the two phases. Composition and structural analysis with EDS and SAD confirmed that the white precipitates are Mg_2Si precipitates (cF12 structure). The large black features (~1 μm) in image B are identified as the Fe-Al rich phase, which has an estimated $FeAl_{5.3}$ composition from EDS measurement. However, the SAD data indicates that the structure does not match that for $FeAl_6$. The small black precipitates in image B and D are an Al-Cr-Mn-Fe compound with a composition of approximately $Al_{87}(Cr, Mn, Fe)_{13}$. The short white arrows in Fig. 19(C) mark the large thin platelet precipitates located in the Al right next to the boundary line between Al and Al_3Mg_2 phase. These are the Mg-rich precipitates residing on the (100) plane of fcc Al and their exact composition and structure cannot be determined from this work due to limitations of the instrument. Fig. 20 shows the SAD zone pattern in the Al at [100] (left) and the bright field images of the large Mg-rich platelet precipitates at [100] (middle). After tilting toward the 10 o'clock direction for 24° (right), the thin

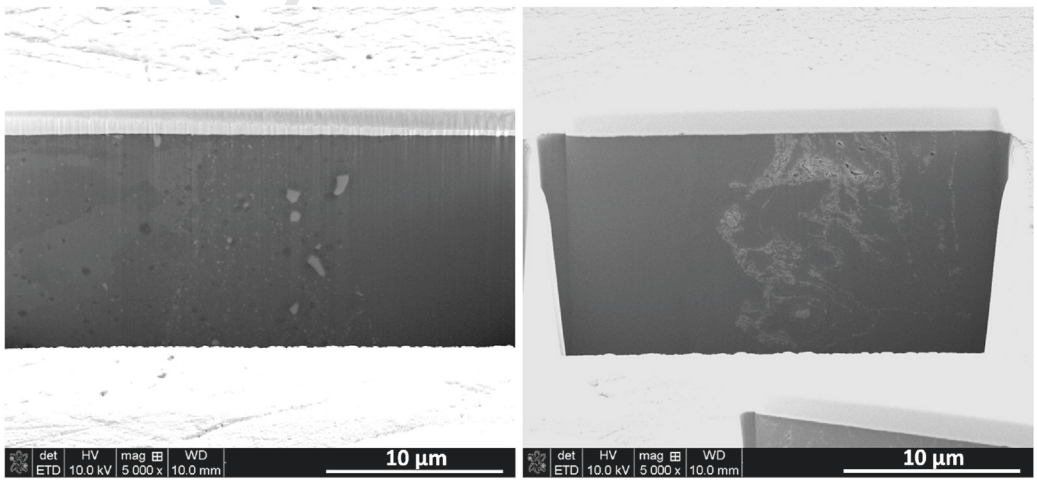

Fig. 18. SEM low magnification images of sectional view of site G (left) and site H (right) at the interface of Mg matrix and Al cladding from low fission density sample (3.7×10^{21} f/cm^3).

Please cite this article in press as: J. Gan, et al., TEM characterization of irradiated U-7Mo/Mg dispersion fuel, Journal of Nuclear Materials (2017), http://dx.doi.org/10.1016/j.jnucmat.2017.07.030

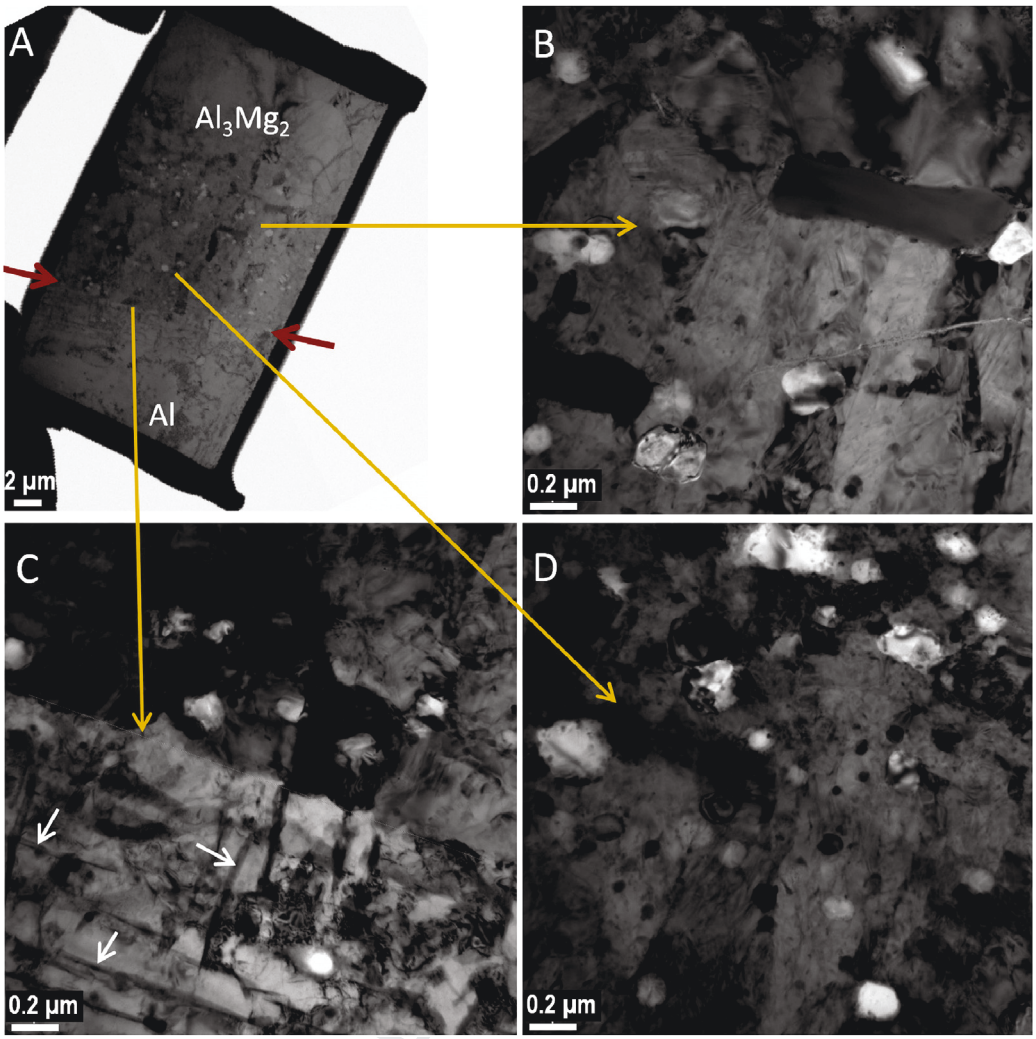

Fig. 19. TEM low magnification overview of site G lamella (A) with red arrows marking the interface between Al and Al_3Mg_2, and three detailed views at higher magnification from the transition areas marked by the long lines from low fission density sample (3.7×10^{21} f/cm^3). The white arrows in Al mark the Mg-rich large thin platelet precipitates in Al (100) planes near the interface between Al and Al_3Mg_2 (C). See text for details on other precipitates shown in picture (B) and (D). (For interpretation of the references to colour in this figure legend, the reader is referred to the web version of this article.)

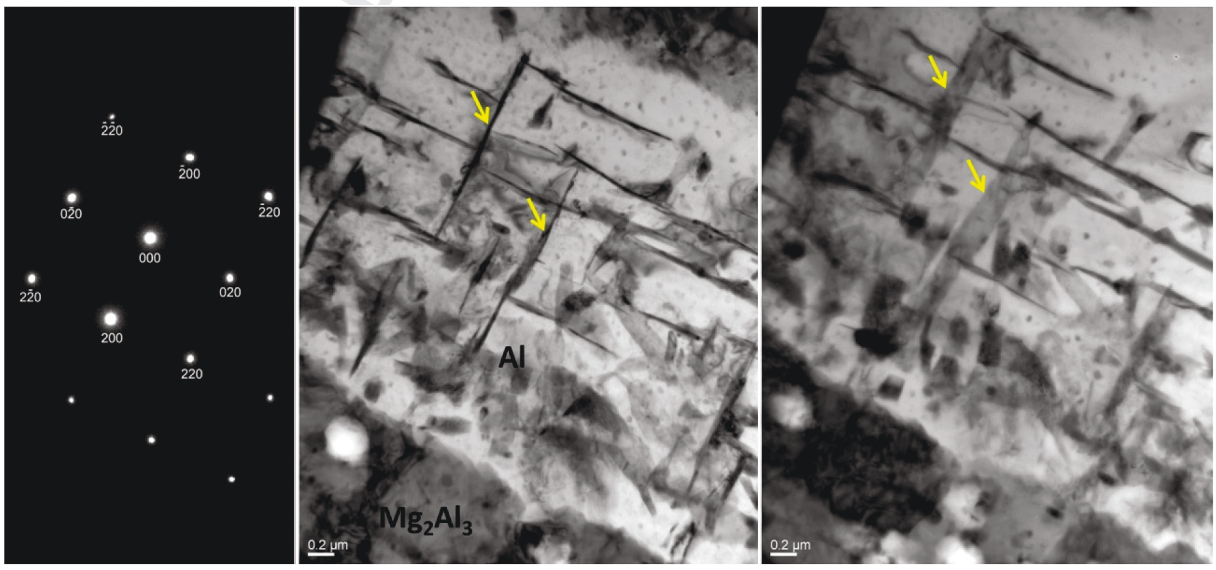

Fig. 20. TEM images of SAD zone [100] in Al (left) near Al-Al_3Mg_2 interface showing Mg-rich large platelet precipitates at [100] (middle) and after tilt to the 10 o'clock direction for 24° (right).

Please cite this article in press as: J. Gan, et al., TEM characterization of irradiated U-7Mo/Mg dispersion fuel, Journal of Nuclear Materials (2017), http://dx.doi.org/10.1016/j.jnucmat.2017.07.030

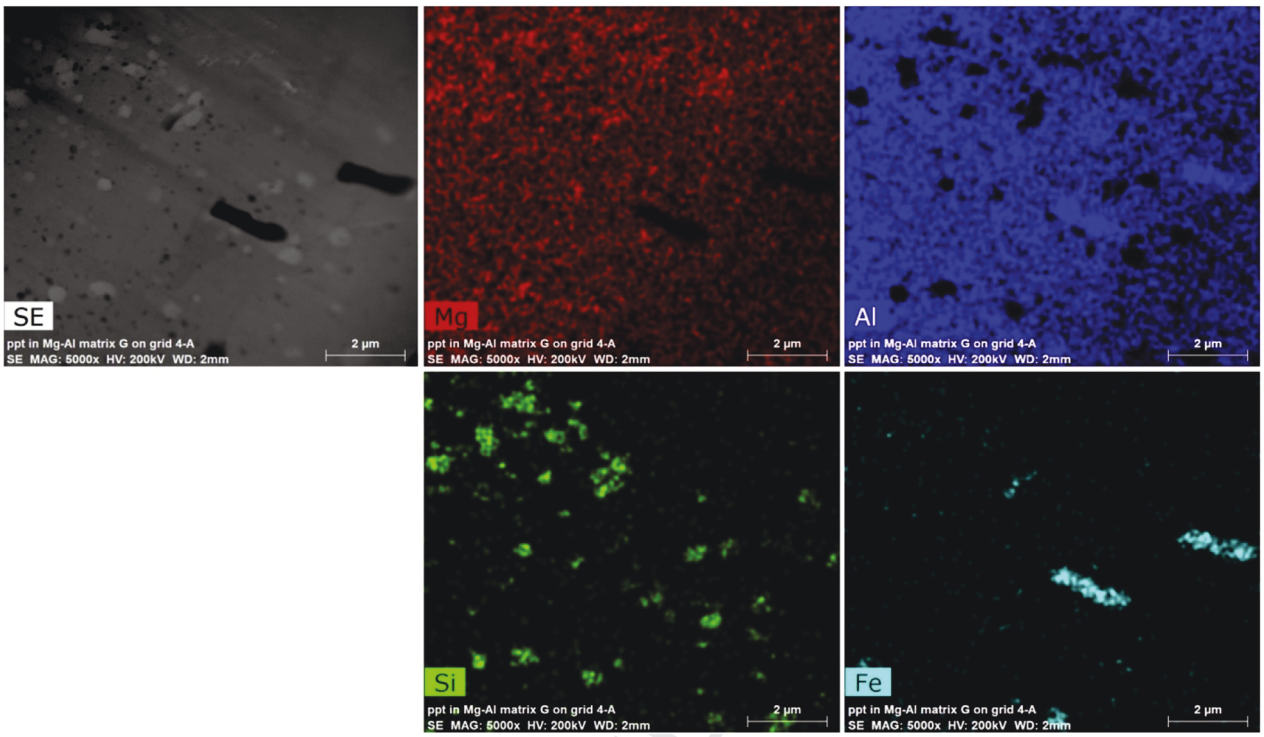

Fig. 21. STEM image and EDS mapping showing various types of precipitates in Al_3Mg_2 near Al cladding and Mg matrix interface in site G lamella at low fission density (3.7×10^{21} f/cm^3).

platelet characteristic of these large precipitates with size up to ~ 1 μm can be revealed. A low-resolution EDS elemental map from site G TEM lamella is shown in Fig. 21. It clearly shows the large black precipitates are enriched in Fe and Al, the white precipitates are enriched in Mg and Si, and the small black precipitates are Fe-rich.

A TEM low magnification overview and an intermediate magnification image for site H lamella are shown in Fig. 22. The red dashed line marks approximately the boundary between Al_3Mg_2 phase (cF1832 structure) and $Al_{12}Mg_{17}$ phase (cI58 structure). The feature with slightly dark contrast and small black dots are identified to be MgO by EDS measurement. The white features are either a perforation in irregular shape or extremely thin areas. These areas with high concentration of MgO in $Al_{12}Mg_{17}$ phase are likely the result of oxygen contamination from fuel fabrication. Fig. 23 shows the STEM image from a region near the edge of the site H sample, where the arrowed line shows the EDS line scan along with the x-ray intensity profile that reveals the composition changes as one moves through the MgO, the $Al_{12}Mg_{17}$ and Al_3Mg_2 phases.

Fig. 24 reveals the low magnification TEM overview of site I lamella with EDS spectrum from 5 areas (a – e). The spectrums

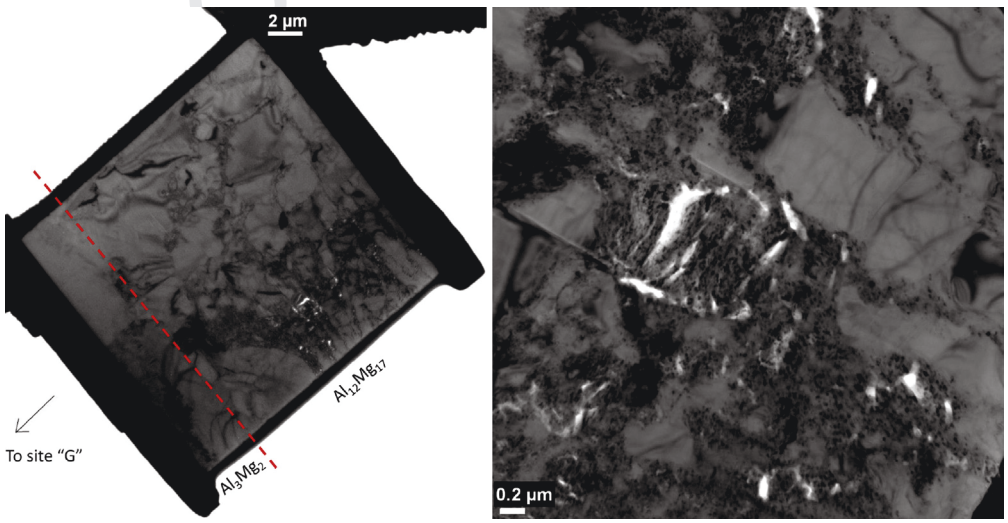

Fig. 22. TEM low magnification overview view of site H (left) and the detailed view at high magnification (right) from low fission density sample (3.7×10^{21} f/cm^3).

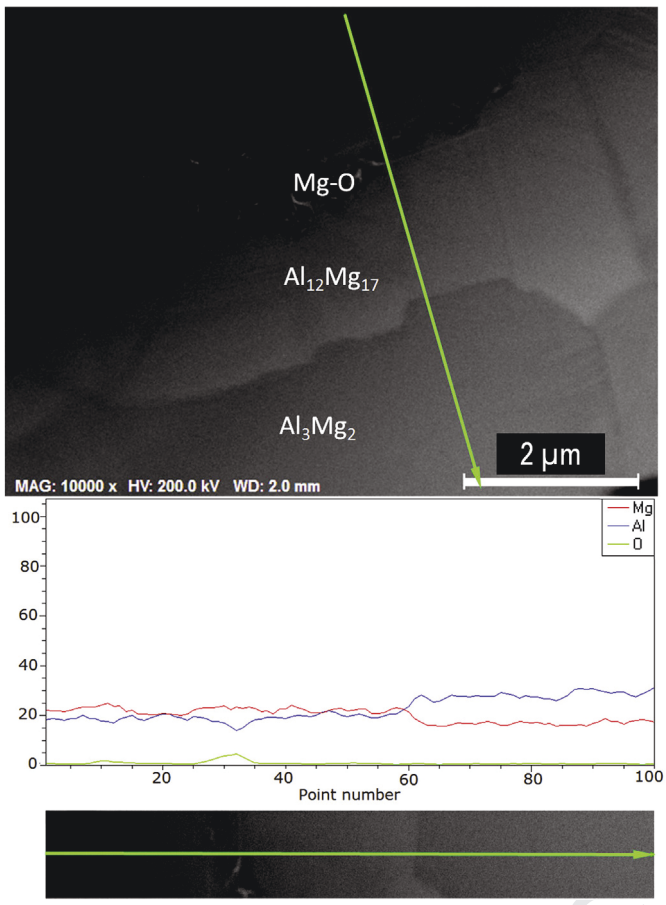

Fig. 23. STEM image of site H (top) from low fission density sample (3.7×10^{21} f/cm^3) and the x-ray intensity profile of elemental line scan showing the presence of Mg-O and the transition between $Al_{12}Mg_{17}$ and Al_3Mg_2 phase.

indicate a transition from $M_{17}Al_{12}$ at a, b and c to Mg at d and e. By combining all the information from 3 TEM lamellas (G, H and I) taken from the low fission density sample, it is possible to show that the reaction layer between Al alloy cladding and Mg matrix is approximately 70 μm thick with a transition sequence of Al → Al_3Mg_2 → $Al_{12}Mg_{17}$ → Mg. The reaction layer thickness for the Al_3Mg_2 phase seems larger than that for the $Al_{12}Mg_{17}$ phase. Fig. 25 shows the TEM bright field images at g = 3–30 in the $Al_{12}Mg_{17}$ phase at both low and high magnifications. High concentration stacking faults and spotty features are clearly visible. These spotty features are likely small MgO precipitates similar to that shown in Fig. 22. Comparing to the reaction phases identified in the Mg-Al6061 diffusion couple work by Kammerer et al. [14], a thin layer of $Al_{30}Mg_{23}$ phase was not found between Al_3Mg_2 and $Al_{12}Mg_{17}$ in the irradiated Mg-matrix U(Mo) dispersion fuel. One possible explanation is that this phase may not be stable under irradiation hence its nucleation and growth is inhibited in the irradiation fuel.

At high fission density of 5.5×10^{21} f/cm^3, an enlarged edge-on view of the site X, Y and Z from KGT-1222 sample is shown in Fig. 26. A large fabrication defect can be seen on one side of site Z lamella. It is believed that this type of defects introduced from fuel fabrication can be effectively mitigated through optimization of fabrication process control. Fig. 27 shows a montage of low magnification TEM images from site X, Y and Z. It is evident that these three lamellas, crossing a length of approximately 55 μm,

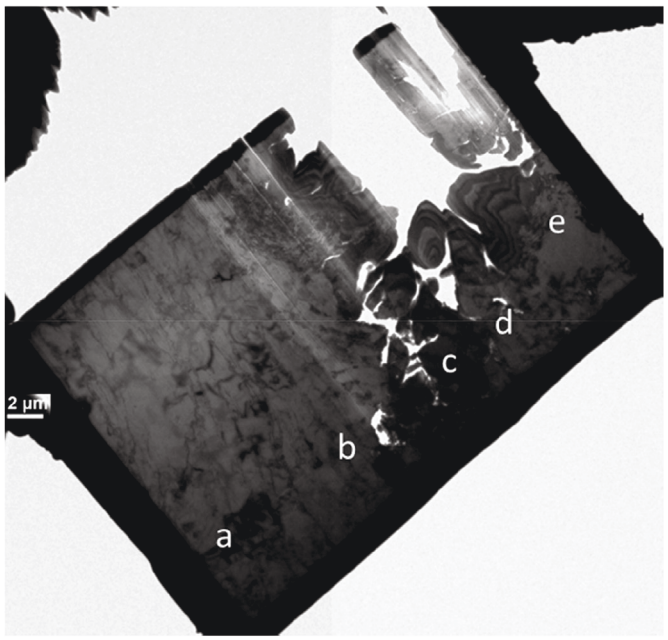

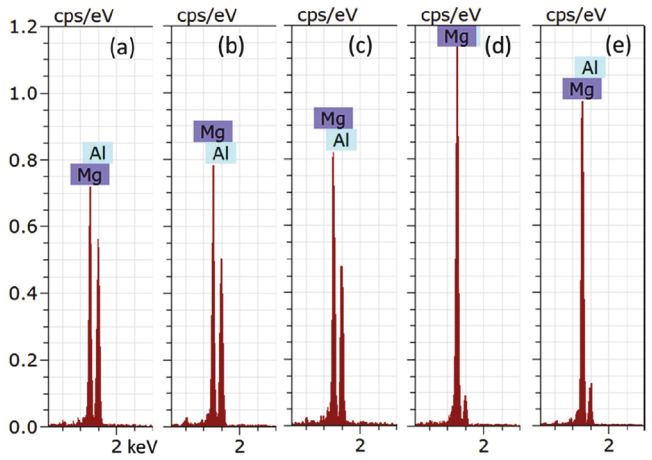

Fig. 24. STEM image of site I (top) and the EDS spectrum showing the transition from $Al_{12}Mg_{17}$ (a, b and c) to Mg phase (d and e).

only capture a portion of the transitional microstructure at the interface of Mg matrix and Al alloy cladding. While phase Al_3Mg_2 and Al are missing in the pictures, a large area of carbon is identified by EDS measurement in site Y and Z lamellas. The unexpected presence of carbon is likely introduced as a result of material contamination. Comparing to the interface microstructure in the transition from Mg to $Al_{12}Mg_{17}$ for low fission density sample (KGT-1225), the microstructure in the similar transition region for the high fission density sample (KGT-1222) is more complex. It appears that this transition microstructure consists of (1) Mg, (2) Mg with $Al_{12}Mg_{17}$ precipitates, (3) a mixture of (2) plus $Al_{12}Mg_{17}$ phase, and (4) $Al_{12}Mg_{17}$ phase. Fig. 28 shows an enlarged view of site X lamella from region in the upper right corner with EDS line scan from $Al_{12}Mg_{17}$ phase to Mg phase with $Al_{12}Mg_{17}$ precipitates. It is not clear whether this difference in transitional microstructure at Mg-Al interface region is from inhomogeneity in the fresh fuel microstructure or from radiation effect at high fission density. Since Al_3Mg_2 is not captured in site Z lamella, whether a thin layer of $Al_{30}Mg_{23}$ phase is present between Al_3Mg_2 and $Al_{12}Mg_{17}$ phase for

Please cite this article in press as: J. Gan, et al., TEM characterization of irradiated U-7Mo/Mg dispersion fuel, Journal of Nuclear Materials (2017), http://dx.doi.org/10.1016/j.jnucmat.2017.07.030

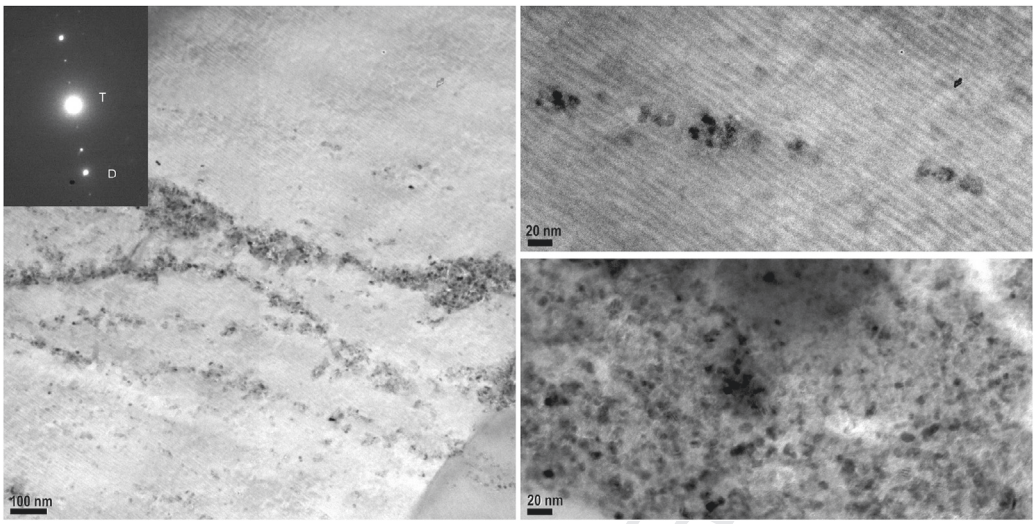

Fig. 25. TEM bright field image at g = 3–30 in $Al_{12}Mg_{17}$ (cI58 structure) at low (left) and high (right) magnification revealing high concentration stacking faults (top-right) and spotty features (bottom-right) for site I lamella at 3.7 × 10^{21} f/cm^3.

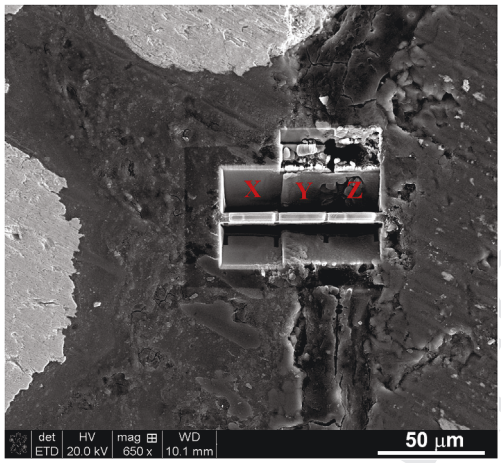

Fig. 26. FIB SEM image of site X, Y and Z at the interface of Mg matrix and Al alloy cladding for the high fission density sample (5.5 × 10^{21} f/cm^3).

the high fission density fuel cannot be verified in this work.

Overall, the characterized phases at the fuel meat (U-7Mo with Mg matrix)/Al alloy cladding interface for both the low and high-fission density samples did not exhibit regions with large porosity. It appeared that the phases present in the interaction zone exhibited good radiation stability and remained crystalline.

4. Summary

TEM characterization of the irradiated U(Mo)/Mg dispersion fuel plate with Al6061 cladding reveal complex transitional microstructure at Mg-Al alloy interface with no evidence of Mg-U(Mo) interaction at the interface between Mg matrix and U(Mo) fuel particles. The microstructure of the U(Mo) fuel particles between Mg matrix and Al alloy matrix is in general consistent except the former shows much less large bubbles near fuel particle surface region. This further improves heat conduction for fuel particles in addition to the absence of FMI.

At fission density of 3.7 × 10^{21} f/cm^3, the interaction layer at Al

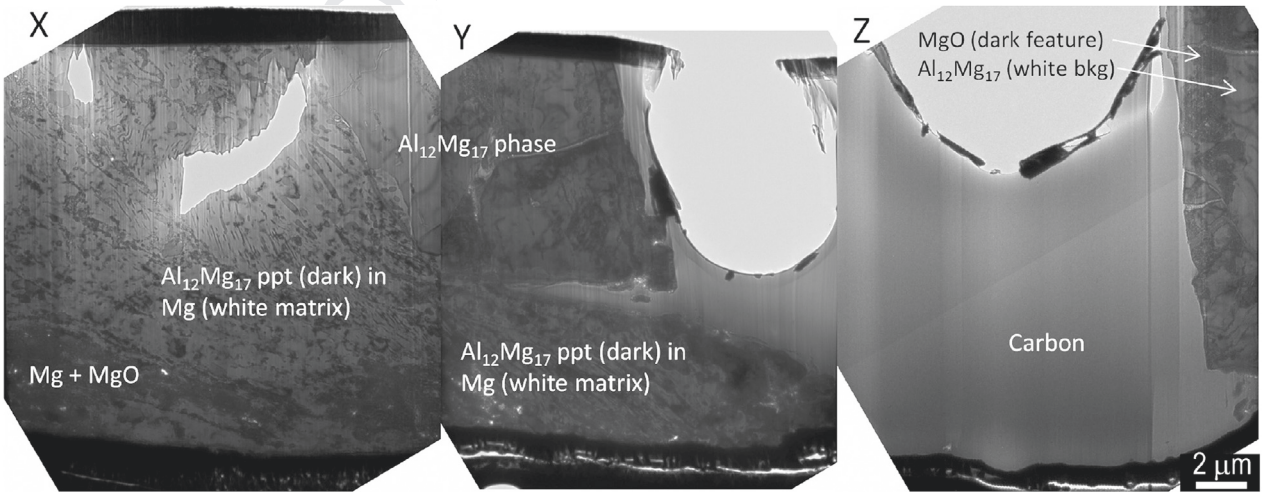

Fig. 27. A TEM montage image of low magnification overview of site X, Y and Z at the interface of Mg matrix and Al alloy cladding for sample at a high fission density of 5.5 × 10^{21} f/cm^3.

Please cite this article in press as: J. Gan, et al., TEM characterization of irradiated U-7Mo/Mg dispersion fuel, Journal of Nuclear Materials (2017), http://dx.doi.org/10.1016/j.jnucmat.2017.07.030

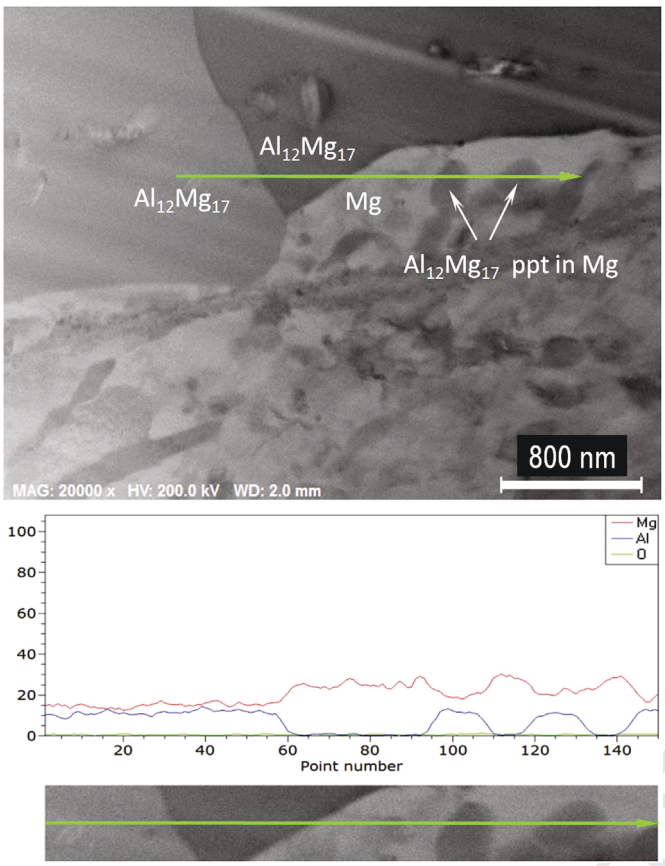

Fig. 28. A STEM image and EDS line scan at Mg - Al interface region (site X) at a fission density of 5.5 × 10^{21} f/cm^3 revealing transition from $Al_{12}Mg_{17}$ phase (left) to Mg (right) including $Al_{12}Mg_{17}$ precipitates shown in dark contrast.

alloy cladding and Mg matrix consists of Al→Al_2Mg_3 (~30 μm)→$Al_{12}Mg_{17}$ (~20 μm)→Mg. The complex cubic phase Al_2Mg_3 (1832 atoms) contains low concentration stacking faults while the less complex cubic phase $Al_{12}Mg_{17}$ (58 atoms) reveals very high density of stacking faults. The $Al_{12}Mg_{17}$ phase contains MgO precipitates shown as irregular or spotty features with dark contrast. The Mg_2Si precipitates (200–1000 nm) are shown as white feature mainly in Al_3Mg_2 phase within 10 μm from the Al/Al_3Mg_2 interface. Other type precipitates at the Al-Mg interface region include low density large $FeAl_{5.3}$ precipitates (up to 1 μm) and high density small precipitates (Al-Cr-Mn-Fe) in Al_2Mg_3 and Mg-rich large thin platelet precipitates in Al. A thin lay (~200 nm) with slightly gray contrast right next to the U(Mo) fuel particle surface is likely caused by radiation-induced mixing. The interior microstructure of U(Mo) fuel particles reveals a correlation of higher Mo with relatively clean microstructure and lower Mo with more pronounced large bubble development. The small elongated bubbles wrapping around the clean area suggests that bubble coalescence is an important mechanism to convert GBS to large bubbles. The clean areas consist of fine GBS bubbles of approximately 3.5 nm with a GBS constant of 11.2 nm of fcc structure, consistent to that found in the previous work at relevant fission densities.

At high fission density of 5.5 × 10^{21} f/cm^3, the complex transitional microstructure at the Mg-Al alloy interface appears further developed with coexisting of $Al_{12}Mg_{17}$ phase and elongated $Al_{12}Mg_{17}$ precipitates in Mg matrix. No convincible evidence of U(Mo) and Mg interaction product can be found. The radiation mixing appears enhanced at some surface region of U(Mo) and agglomeration of U(Mo) in Mg becomes evident. In the U(Mo) fuel particle interior, subdivided grains with few hundred nm and small misfit angles are identified with no sign of large bubble development at those boundaries. Small pockets of residual GBS are still present with bubble size and GBS constant similar to that found at low fission density.

U. S. Department of Energy disclaimer

Acknowledgments

This work was supported by the U.S. Department of Energy, Office of Nuclear Materials Threat Reduction (NA-212), National Nuclear Security Administration, under DOE-NE Idaho Operations Office Contract DE-AC07-05ID14517. This manuscript was authored by a contractor for the U.S. Government. The U.S. Government retains and the publisher, by accepting the article for publication, acknowledges that the U.S. Government retains a nonexclusive, paid-up, irrevocable, worldwide license to publish or reproduce the published form of this manuscript, or allow others to do so, for U.S. Government purposes.

References

[1] G. Hofman, M. Meyer, in: Proceedings of the 21st International Meeting on Reduced Enrichment for Research and Test Reactors (RERTR), Sao Paulo, 1998.
[2] M. Meyer, G. Hofman, S. Hayes, C. Clark, T. Wiencek, J. Snelgrove, R. Strain, K.-H. Kim, J. Nucl. Mater. 304 (2002) 221–236.
[3] D. Wachs, D. Keiser, M. Meyer, D. Burkes, C. Clark, G. Moore, J. Jue, M. Finlay, T. Totev, G. Hofman, T. Wiencek, Y. Kim, J. Snelgrove, in: Proceedings of 7th Int. Conf. on Adv. Nucl. Fuel Cycles and Systems, GLOBAL 2007, Boise, ID, September 9-13, 2007, p. 1322.
[4] A. Leenaers, S. Van den Berghe, E. Koonen, C. Jarousse, F. Huet, M. Trotabas, M. Boyard, S. Guillot, L. Sannen, M. Verwerft, J. Nucl. Mater 335 (2004) 39–47.
[5] S. Van den Berghe, W. Van Renterghem, A. Leenaers, J. Nucl. Mater 375 (2008) 340.
[6] Y.S. Kim, G. Hofman, J. Nucl. Mater 425 (2011) 181–187.
[7] Y.S. Kim, G.L. Hofman, H.J. Ryu, J. Rest, in: Proc. of the RERTR-2005 International Meeting, Boston, MA, 2005.
[8] D.D. Keiser Jr., J.F. Jue, J. Gan, A.B. Robinson, P. Medvedev, B. Miller, D.M. Wachs, in: Proc. of the RERTR-2010 International Meeting, Lisbon, Portugal, 2010.
[9] S. Van den Berghe, A. Leenaers, E. Koonen, L. Sannen, Adv. Sci. Technol. 73 (2010) 78–90.
[10] S. Van den Berghe, A. Leenaers, C. Detavernier, in: Proceedings of the International Topical Meeting on Research Reactor Fuel Management (RRFM), Rome, 2011.
[11] A. Leenaers, S. Van den Berghe, C. Detavernier, in: Proceedings of the International Topical Meeting on Research Reactor Fuel Management (RRFM), Rome, 2011.
[12] D.D. Keiser Jr., J.-F. Jue, B.D. Miller, J. Gan, A.B. Robinson, P.G. Medvedev, J.M. Madden, G.A. Moore, Metallurgical Mater. Trans. E 3E (2016) 71–89.
[13] H.-Y. Chiang, M. Doblinger, S.-H. Park, L. Beck, W. Petry, J. Nucl. Mater 453 (2014) 41–47.
[14] C.C. Kammerer, M. Fu, L. Zhou, D.D. Keiser Jr., Y.H. Sohn, Defect Diffus. Forum 364 (2015) 174–181.
[15] K. Huang, H. Heinrich, D.D. Keiser Jr., Y.H. Sohn, Defect Diffusion Forum 333 (2013) 199–206.
[16] N. Wang, M. Kulakov, S. Hibbins, in: International Topical Meeting on

Research Reactor Fuel Management (RRFM), Bucharest, Romania, 2015 April 19-23.
[17] Mykola Kulakov, Mouna Saoudi, Markus H.A. Piro, Ronald L. Donaberger, J. Nucl. Mater 484 (2017) 288–296.
[18] J. Gan, B.D. Miller, D.D. Keiser Jr., A.B. Robinson, J.W. Madden, P.G. Medvedev, D.M. Wachs, J. Nucl. Mater. 454 (2014) 434–445.
[19] Hj Matzke, H. Blank, J. Nucl. Mater. 166 (1989) 120.
[20] J. Gan, D.D. Keiser Jr., D.M. Wachs, A.B. Miller, T.R. Allen, J. Nucl. Mater. 396 (2010) 234–239.
[21] J. Gan, D.D. Keiser Jr., B.D. Miller, A.B. Robinson, J.F. Jue, P. Medvedev, D.M. Wachs, J. Nucl. Mater 424 (2012) 43–50.
[22] R. Jungwirth, T. Zweifel, H.-Y. Chiang, W. Petry, S. Van den Berghe, A. Leenaers, J. Nucl. Mater. 434 (2013) 296–302.

Please cite this article in press as: J. Gan, et al., TEM characterization of irradiated U-7Mo/Mg dispersion fuel, Journal of Nuclear Materials (2017), http://dx.doi.org/10.1016/j.jnucmat.2017.07.030